

RL-TR-96-128  
Final Technical Report  
July 1996



# ROBUST LOCALLY OPTIMUM DETECTION

Illinois Institute of Technology

Donald R. Ucci, William E. Jacklin, and Myron R. Mychal

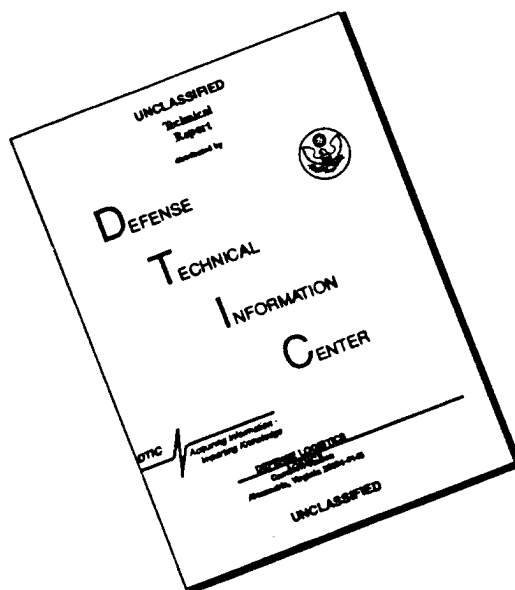
DTIC QUALITY INSPECTED 21

*APPROVED FOR PUBLIC RELEASE; DISTRIBUTION UNLIMITED.*

19961001 005

Rome Laboratory  
Air Force Materiel Command  
Rome, New York

# DISCLAIMER NOTICE

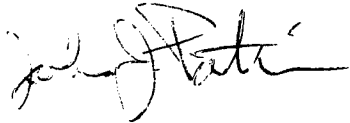


**THIS DOCUMENT IS BEST QUALITY AVAILABLE. THE COPY FURNISHED TO DTIC CONTAINED A SIGNIFICANT NUMBER OF PAGES WHICH DO NOT REPRODUCE LEGIBLY.**

This report has been reviewed by the Rome Laboratory Public Affairs Office (PA) and is releasable to the National Technical Information Service (NTIS). At NTIS, it will be releasable to the general public, including foreign nations.

RL-TR- 96-128 has been reviewed and is approved for publication.

APPROVED:



JOHN J. PATTI  
Project Engineer

FOR THE COMMANDER:



JOHN A. GRANIERO  
Chief Scientist  
Command, Control & Communications Directorate

If your address has changed or if you wish to be removed from the Rome Laboratory mailing list, or if the addressee is no longer employed by your organization, please notify Rome Laboratory/ ( C3BB), Rome NY 13441. This will assist us in maintaining a current mailing list.

Do not return copies of this report unless contractual obligations or notices on a specific document require that it be returned.

# REPORT DOCUMENTATION PAGE

Form Approved  
OMB No. 0704-0188

Public reporting burden for this collection of information is estimated to average 1 hour per response, including the time for reviewing instructions, searching existing data sources, gathering and maintaining the data needed, and completing and reviewing the collection of information. Send comments regarding this burden estimate or any other aspect of the collection of information, including suggestions for reducing this burden, to Washington Headquarters Service, Directorate for Information Operations and Reports, 1215 Jefferson Davis Highway, Suite 1204, Arlington, VA 22202-4302, and to the Office of Management and Budget, Paperwork Reduction Project (0704-0188), Washington, DC 20503.

1. AGENCY USE ONLY (Leave Blank)		2. REPORT DATE July 1996		3. REPORT TYPE AND DATES COVERED Final ----	
4. TITLE AND SUBTITLE  ROBUST LOCALLY OPTIMUM DETECTION				5. FUNDING NUMBERS C - F30602-94-C-0148 PE - 62702F PR - 4519 TA - 42 WU - PH	
6. AUTHOR(S)  Donald R. Ucci, William E. Jacklin, and Myron R. Mychal					
7. PERFORMING ORGANIZATION NAME(S) AND ADDRESS(ES) Illinois Institute of Technology Department of Electrical & Computer Engineering 3300 South Federal St. Chicago IL 60616-3793				8. PERFORMING ORGANIZATION REPORT NUMBER  N/A	
9. SPONSORING/MONITORING AGENCY NAME(S) AND ADDRESS(ES)  Rome Laboratory/C3BB 525 Brooks Rd Rome NY 13441-4505				10. SPONSORING/MONITORING AGENCY REPORT NUMBER  RL-TR-96-128	
11. SUPPLEMENTARY NOTES  Rome Laboratory Project Engineer: John J. Patti/C3BB/(315) 330-3615					
12a. DISTRIBUTION/AVAILABILITY STATEMENT  Approved for public release; distribution unlimited.				12b. DISTRIBUTION CODE	
13. ABSTRACT (Maximum 200 words) The Locally Optimum (LO) detection technique has been studied for the improvement of communication system performance, especially for spread spectrum systems, wherein performance can still be degraded by high interference to signal ratios. A wide variety of signal interference types can be handled using advanced statistical decision and signal processing techniques, resulting in a robust receiver, suitable for incorporation into the SMART radio system. Two specific detectors are reviewed, namely the histogram indirect and the Fourier series approximation direct methods. Three associated LO detector enhancement techniques are derived and examined: the Least Squares (LS); the Characteristic Function (CF); and the preamble enhancement methods. Based on simulations developed using MATLAB, the enhanced LO detectors are shown to provide, in most cases, significantly better performance than previous methods. Moreover, the preamble technique is shown to be much more robust than the LS and CF enhancement methods, the cost being an increase in system overhead, something that is usually mostly already paid for by other system acquisition and protocol functions.					
14. SUBJECT TERMS Communications, Signal processing, Signal detection, Spread spectrum				15. NUMBER OF PAGES 44	
				16. PRICE CODE	
17. SECURITY CLASSIFICATION OF REPORT UNCLASSIFIED		18. SECURITY CLASSIFICATION OF THIS PAGE UNCLASSIFIED		19. SECURITY CLASSIFICATION OF ABSTRACT UNCLASSIFIED	
				20. LIMITATION OF ABSTRACT UL	

# Contents

<b>Executive Summary</b>	<b>8</b>
<b>1 Introduction</b>	<b>9</b>
<b>2 Robust LO Detection</b>	<b>11</b>
2.1 The Histogram Robust LO Detector . . . . .	12
2.2 The Direct FSA Robust LO Detector . . . . .	14
<b>3 Enhancement Techniques</b>	<b>17</b>
3.1 The Least Squares Method . . . . .	17
3.1.1 The LS Enhanced BPSK LO Detector for Independent Noise . . . . .	19
3.1.2 Sample Operation . . . . .	21
3.2 The Characteristic Function Method . . . . .	23
3.2.1 The CF Enhanced BPSK LO Detector for Independent Noise . . . . .	28
3.2.2 Sample Operation . . . . .	28
3.3 The Preamble Method . . . . .	29
3.3.1 The Preamble Method and the FSA LO Detector . . .	36
3.3.2 The Preamble Method and the Histogram LO Detector	38
3.3.3 The Variance of the Estimator $\hat{\Phi}_n(k\omega_0)$ . . . . .	48
<b>4 Performance Analysis</b>	<b>53</b>
4.1 Results for the Histogram Robust LO Detector . . . . .	54
4.1.1 The LS Enhancement Technique . . . . .	54
4.1.2 The CF Enhancement Technique . . . . .	58
4.1.3 The Preamble Enhancement Technique . . . . .	61

4.2	Results for the FSA Robust LO Detector . . . . .	62
4.2.1	The CF Enhancement Technique . . . . .	63
4.2.2	The Preamble Enhancement Technique . . . . .	66
<b>5</b>	<b>Summary and Future Research</b>	<b>70</b>
5.1	Summary . . . . .	70
5.2	Future Research . . . . .	71
	<b>Bibliography</b>	<b>75</b>

# List of Figures

3.1	A typical least squares filtering problem. . . . .	19
3.2	Histogram estimate of the received signal pdf, $K = 99$ , $T = 200$ , $E_c/\sigma = 8 \text{ dB}$ . . . . .	23
3.3	Histogram estimate of the noise pdf, $K = 99$ , $T = 200$ , $E_c/\sigma = 8 \text{ dB}$ . . . . .	24
3.4	LS enhanced histogram estimate of the noise signal pdf, $K = 99$ , $T = 200$ , $E_c/\sigma = 8 \text{ dB}$ , $L = 50$ . . . . .	24
3.5	Histogram estimate of the LO nonlinearity using noise samples, $K = 99$ , $T = 200$ , $E_c/\sigma = 8 \text{ dB}$ . . . . .	25
3.6	LS enhanced histogram estimate of the LO nonlinearity, $K = 99$ , $T = 200$ , $E_c/\sigma = 8 \text{ dB}$ , $L = 50$ . . . . .	25
3.7	Comparison of the two LO nonlinearity estimates, $K = 99$ , $T = 200$ , $E_c/\sigma = 8 \text{ dB}$ , $L = 50$ . Legend: — LS enhancement, . . . Estimate using noise samples . . . . .	26
3.8	The LS deconvolution filter, $K = 99$ , $T = 200$ , $E_c/\sigma = 8 \text{ dB}$ , $L = 50$ . . . . .	27
3.9	Histogram estimate of the received signal pdf, $K = 33$ , $T = 50$ , $E_c/\sigma = -1 \text{ dB}$ . . . . .	30
3.10	Histogram estimate of the noise pdf, $K = 33$ , $T = 50$ , $E_c/\sigma = -1 \text{ dB}$ . . . . .	30
3.11	CF enhanced histogram estimate of the noise signal pdf, $K = 33$ , $T = 50$ , $E_c/\sigma = -1 \text{ dB}$ . . . . .	31
3.12	Histogram estimate of the LO nonlinearity using noise samples, $K = 33$ , $T = 50$ , $E_c/\sigma = -1 \text{ dB}$ . . . . .	31
3.13	CF enhanced histogram estimate of the LO nonlinearity, $K = 33$ , $T = 50$ , $E_c/\sigma = -1 \text{ dB}$ . . . . .	32

3.14	Comparison of the two LO nonlinearity estimates, $K = 33$ , $T = 50$ , $E_c/\sigma = -1$ dB. Legend: — CF enhancement, ... Estimate using noise samples . . . . .	33
3.15	Estimate of the histogram DFT using the CF technique, $K =$ $33$ , $T = 50$ , $E_c/\sigma = -1$ dB. Legend: — CF enhancement, ... Theoretical . . . . .	34
3.16	FSA LO nonlinearity estimated using noise samples, $p = 10$ , $T = 50$ , $Q = 20,000$ , $E_c/\sigma = 0$ dB. . . . .	37
3.17	FSA LO nonlinearity estimated using received signal samples, $p = 10$ , $T = 50$ , $Q = 20,000$ , $E_c/\sigma = 0$ dB. . . . .	37
3.18	FSA LO nonlinearity estimated using the preamble technique, $p = 10$ , $T = 50$ , $Q_2 = 20,000$ , $E_c/\sigma = 0$ dB. . . . .	38
3.19	Estimate of the noise CF using the preamble technique, $p =$ $10$ , $T = 50$ , $Q = 60,000$ ( $Q_2 = 20,000$ ), $E_c/\sigma = 0$ dB. Leg- end: — Preamble technique, ... Theoretical . . . . .	39
3.20	Histogram estimate of the received signal pdf, $K = 15$ , $T =$ $30$ , $Q = 20,000$ , $E_c/\sigma = 0$ dB. . . . .	44
3.21	Histogram estimate of the noise pdf, $K = 15$ , $T = 30$ , $Q =$ $20,000$ , $E_c/\sigma = 0$ dB. . . . .	44
3.22	Preamble enhanced histogram estimate of the noise pdf, $K =$ $15$ , $T = 30$ , $M = 1$ , $Q = 20,000$ , $E_c/\sigma = 0$ dB. . . . .	45
3.23	Histogram estimate of the LO nonlinearity using noise sam- ples, $K = 15$ , $T = 30$ , $Q = 20,000$ , $E_c/\sigma = 0$ dB. . . . .	45
3.24	Histogram estimate of the LO nonlinearity using received sig- nal samples, $K = 15$ , $T = 30$ , $Q = 20,000$ , $E_c/\sigma = 0$ dB. . . .	46
3.25	Preamble enhanced histogram estimate of the LO nonlinearity, $K = 15$ , $T = 30$ , $M = 1$ , $Q = 20,000$ , $E_c/\sigma = 0$ dB. . . . .	46
3.26	Estimate of the histogram DFT using the preamble technique, $K = 15$ , $T = 30$ , $M = 1$ , $Q = 20,000$ , $E_c/\sigma = 0$ dB. Legend: — Preamble enhancement, ... Theoretical . . . . .	47
3.27	Number of samples, $Q$ , required relative to the FSA order, $p$ , indicated by the preamble technique variance criterion. Leg- end: — Cauchy noise, - - Gaussian noise, ... Laplace noise . .	52



4.1	$P_b$ curves for the LS enhanced histogram LO detector with $N = 10$ samples per bit, $K = 33$ histogram bins, filter length $2L - 1 = 99$ , truncation width of $T = 100$ , and $Q = 50,000$ samples per pdf approximation. . . . .	55
4.2	$P_b$ curves for the LS enhanced histogram LO detector with $N = 10$ samples per bit, $K = 33$ histogram bins, filter length $2L - 1 = 99$ , truncation width of $T = 200$ , and $Q = 50,000$ samples per pdf approximation. . . . .	55
4.3	$P_b$ curves for the LS enhanced histogram LO detector with $N = 10$ samples per bit, $K = 99$ histogram bins, filter length $2L - 1 = 199$ , truncation width of $T = 200$ , and $Q = 50,000$ samples per pdf approximation. . . . .	56
4.4	$P_b$ curves for the LS enhanced histogram LO detector with $N = 10$ samples per bit, $K = 99$ histogram bins, filter length $2L - 1 = 199$ , truncation width of $T = 400$ , and $Q = 50,000$ samples per pdf approximation. . . . .	56
4.5	$P_b$ curves for the LS enhanced histogram LO detector with $N = 10$ samples per bit, $K = 99$ histogram bins, filter length $2L - 1 = 199$ , truncation width of $T = 600$ , and $Q = 50,000$ samples per pdf approximation. . . . .	57
4.6	Legend for the probability of bit error figures. . . . .	57
4.7	Effect of bit amplitude position on $P_b$ for the LS enhanced robust LO detector. . . . .	58
4.8	$P_b$ curves for the CF enhanced histogram LO detector with $N = 10$ samples per bit, $K = 99$ histogram bins, truncation width of $T = 200$ , and $Q = 50,000$ samples per pdf approximation. . . . .	59
4.9	$P_b$ curves for the CF enhanced histogram LO detector with $N = 10$ samples per bit, $K = 99$ histogram bins, truncation width of $T = 400$ , and $Q = 50,000$ samples per pdf approximation. . . . .	60
4.10	Effect of bit amplitude position on $P_b$ for the CF enhanced robust LO detector. . . . .	60
4.11	$P_b$ curves for the preamble enhanced histogram LO detector in Cauchy noise with $N = 10$ samples per bit, $K = 33$ histogram bins, truncation width of $T = 100$ , aliasing factor $M = 1$ , and $Q = 50,000$ samples per pdf approximation. . . . .	61

4.12	$P_b$ curves for the preamble enhanced histogram LO detector in Laplace noise with $N = 10$ samples per bit, $K = 15$ histogram bins, truncation width of $T = 30$ , aliasing factor $M = 0$ , and $Q = 20,000$ samples per pdf approximation. . . . .	62
4.13	$P_b$ curves for the preamble enhanced histogram LO detector in Laplace noise with $N = 10$ samples per bit, $K = 15$ histogram bins, truncation width of $T = 30$ , aliasing factor $M = 1$ , and $Q = 20,000$ samples per pdf approximation. . . . .	63
4.14	$P_b$ curves for the CF enhanced FSA LO detector in Cauchy noise with $N = 10$ samples per bit, FSA order of $p = 10$ , truncation width of $T = 50$ and $Q = 20,000$ samples per nonlinearity approximation. . . . .	64
4.15	$P_b$ curves for the CF enhanced FSA LO detector in Cauchy noise with $N = 10$ samples per bit, FSA order of $p = 10$ , truncation width of $T = 100$ and $Q = 20,000$ samples per nonlinearity approximation. . . . .	64
4.16	$P_b$ curves for the CF enhanced FSA LO detector in Cauchy noise with $N = 10$ samples per bit, FSA order of $p = 15$ , truncation width of $T = 100$ and $Q = 20,000$ samples per nonlinearity approximation. . . . .	65
4.17	$P_b$ curves for the preamble enhanced FSA LO detector in Cauchy noise with $N = 10$ samples per bit, FSA order of $p = 10$ , truncation width of $T = 50$ , 20,000 samples per nonlinearity approx. (except preamble), and $Q = 30,000$ training samples (corresponding to $\alpha = 0.00254$ ). . . . .	67
4.18	$P_b$ curves for the preamble enhanced FSA LO detector in Cauchy noise with $N = 10$ samples per bit, FSA order of $p = 10$ , truncation width of $T = 50$ , 20,000 samples per nonlinearity approx. (except preamble), and $Q = 60,000$ training samples (corresponding to $\alpha = 0.00127$ ). . . . .	67
4.19	$P_b$ curves for the preamble enhanced FSA LO detector in Cauchy noise with $N = 10$ samples per bit, FSA order of $p = 15$ , truncation width of $T = 100$ , 20,000 samples per nonlinearity approx. (except preamble), and $Q = 30,000$ training samples (corresponding to $\alpha = 0.000723$ ). . . . .	68

4.20	$P_b$ curves for the preamble enhanced FSA LO detector in Cauchy noise with $N = 10$ samples per bit, FSA order of $p = 15$ , truncation width of $T = 100$ , 20,000 samples per non-linearity approx. (except preamble), and $Q = 60,000$ training samples (corresponding to $\alpha = 0.000361$ ). . . . .	68
4.21	$P_b$ curves for the preamble enhanced FSA LO detector in Laplace noise with $N = 10$ samples per bit, FSA order of $p = 10$ , truncation width of $T = 30$ , 20,000 samples per non-linearity approx. (except preamble), and $Q = 60,000$ training samples (corresponding to $\alpha = 7.96 \times 10^{-5}$ ). . . . .	69

# Executive Summary

Secure and reliable information exchange is essential in military communication systems. However, even in a *spread spectrum* (SS) system, communications can be compromised when the total channel interference power becomes large with respect to that of the desired signal. To improve system performance, one technique that has received considerable attention is robust *locally optimum* (LO) detection in which statistical methods are used to estimate the detector nonlinearity. This report represents the culmination of a study concerning enhancement methods for these types of detectors.

After a brief introduction to the concept of robust LO signal detection, two specific detectors are reviewed, namely, the histogram indirect implementation and the *Fourier series approximation* (FSA) direct implementation. Given this background, three LO detector enhancement techniques are derived and examined: the *least squares* (LS), the *characteristic function* (CF), and the preamble enhancement methods. Based on simulation analyses of various robust LO detector and enhancement combinations, the enhanced LO detectors are shown to provide, in most cases, significantly lower *probability of bit error* ( $P_b$ ) than the corresponding large *jammer-to-signal ratio* ( $J/S$ ) implementation. Moreover, the preamble technique is observed to be immune to the limitations associated with the LS and CF enhancement methods, at the expense of an increase in bandwidth overhead. Finally, a summary and discussion concerning the evolution of this research topic are provided at the conclusion of the report.

# Chapter 1

## Introduction

Secure and reliable information exchange is essential in military communication systems. However, even in a *spread spectrum* (SS) system, communications can be compromised when the total channel interference power becomes large with respect to that of the desired signal. Furthermore, if the channel interference is non-Gaussian, standard linear receiver techniques may exhibit performance degradations since they may no longer be optimal for the given noise environment. In these situations a nonlinear receiver can be used to achieve acceptable and reliable communications.

One method for improving system performance that has received considerable attention, particularly for applications in high *jammer-to-signal ratio* ( $J/S$ ) environments, is *locally optimum* (LO) detection [1]-[4]. In its original form, the LO detector utilizes a nonlinearity derived as an approximation to the optimum *maximum likelihood* (ML) detector. In many scenarios, the LO detector is simpler to implement than the corresponding ML detector, and its performance asymptotically approaches that of the ML detector as the signal becomes small relative to the interference.

One drawback to the original form of the LO detector is that, similar to the ML detector, it requires *a priori* knowledge of the noise *probability density function* (pdf) to implement the detector nonlinearity. Recent efforts have concentrated on the development of *robust* LO detectors that do not require prior knowledge of the interference statistics [5]-[10]. Instead, these detectors attempt to construct estimates of the interference statistics from the available observations. In standard robust LO detection, the required detector is implemented using the received signal samples to estimate the

interference pdf and/or the LO nonlinearity. However, previous work suggests that even in large  $J/S$  environments, the noise samples cannot always be adequately approximated by the received signal samples. Thus, the goal of this research effort is to identify and develop techniques that will enhance the effectiveness of the various LO detector algorithms, particularly where performance degradation has been observed.

The organization of this report is as follows. First, the theoretical LO detector for independent noise and the concept of robust LO detection are introduced in Chapter 2. Additionally, this chapter reviews two types of LO detectors: the histogram indirect implementation method and the *Fourier series approximation* (FSA) direct implementation method. Next, Chapter 3 describes three robust LO detector enhancement techniques in detail. In Chapter 4, performance results for the various robust LO detector and enhancement combinations are presented and compared. Finally, a summary of the research study is provided in Chapter 5, including a discussion concerning the projected evolution of this research topic.

## Chapter 2

# Robust LO Detection

Due to the complexity of the various enhancement algorithms examined, this study focuses on binary detection of real, discrete signals in additive noise. In binary signal detection the goal is to decide which of two possible information signals is present at the detector. For example, in a *binary phased shift keyed* (BPSK) communications system [11], the receiver must decide whether a value of +1 or -1 was sent by the transmitter. Stated more formally, the goal of the detector is to correctly choose one of the following two hypotheses:

$$\begin{aligned} H_1 &: \text{Signal } \mathbf{s}_1 \text{ present} \\ H_0 &: \text{Signal } \mathbf{s}_0 \text{ present,} \end{aligned} \quad (2.1)$$

where  $\mathbf{s}_1$  and  $\mathbf{s}_0$  are vectors and the notation  $\mathbf{x} = [x_1 \cdots x_N]^T$  denotes a vector of length  $N$ . The value of  $N$  is the number of signal samples in a given observation period.

Let the received random signal vector,  $\mathbf{r}$ , be given by

$$\mathbf{r} = \mathbf{s}_m + \mathbf{n}, \quad (2.2)$$

where  $\mathbf{n}$  is the random noise vector, and  $m = 0$  or  $1$ . If  $\rho$  is the actual realization of  $\mathbf{r}$ , and the noise samples are *independent and identically distributed* (iid), then it can be shown [12] that the corresponding LO detector is given by

$$l(\rho) = \sum_{i=1}^N (s_{1i} - s_{0i}) g(\rho_i) \quad \begin{array}{l} \text{choose } H_1 \\ > \\ < \\ \text{choose } H_0 \end{array} \quad \tilde{\gamma}, \quad (2.3)$$

where

$$g(\rho_i) \triangleq -\frac{d}{d\rho_i} \ln[f_n(\rho_i)] = -\frac{f'_n(\rho_i)}{f_n(\rho_i)}, \quad (2.4)$$

and  $f_n(\cdot)$  is the noise pdf. The constant  $\tilde{\gamma}$  is chosen depending on the type of hypothesis test being used [13], e.g., *maximum likelihood* (ML), *maximum a posteriori* (MAP), *Neyman-Pearson* (NP), or general Bayesian. For example, for the case of ML detection of equally likely information signals,  $\tilde{\gamma} = 0$ .

In the *robust* LO detection problem, the noise pdf,  $f_n(\cdot)$ , is unknown. As a result the LO nonlinearity,  $g(\rho_i)$ , must be estimated either directly or indirectly. Indirect methods involve constructing an estimate of the noise pdf,  $\hat{f}_n(\cdot)$ , and using the result to approximate  $g(\rho_i)$  as

$$\hat{g}(\rho_i) = -\frac{d}{d\rho_i} \ln[\hat{f}_n(\rho_i)], \quad (2.5)$$

or

$$\hat{g}(\rho_i) = -\frac{\hat{f}'_n(\rho_i)}{\hat{f}_n(\rho_i)}. \quad (2.6)$$

An example of an indirect method is the histogram implementation of the robust LO detector [6]. Direct methods, on other hand, do not require an intermediate pdf estimate. Rather,  $g(\cdot)$  is estimated directly from the observed data. The direct *Fourier series approximation* (FSA) robust LO detector [14] is one such method.

Whether an indirect or direct method is employed, the underlying LO nonlinearity is a function of the *noise* pdf. As a result, the various robust LO detection algorithms initially assume that uncorrupted observations of the noise samples are available for statistical estimation of the detector. However, in many practical applications the only signal available at the detector is the received signal. Thus, the goal of this research effort is to identify enhancement techniques that allow use of the available received signal for detector estimation while still maintaining acceptable performance.

## 2.1 The Histogram Robust LO Detector

As mentioned previously, the histogram robust LO detector [6] utilizes an indirect approximation of the LO nonlinearity given by Eq. (2.5). In this



method, the available noise observations are assigned to one of  $K$  intervals, and a sample probability is computed for each interval. The resulting histogram pdf estimate is then used to implement the robust LO nonlinearity. More formally, given  $\{\eta_j\}$  as the set of  $Q$  observed samples of the noise random variable,  $n$ , the histogram pdf estimate is given by

$$\hat{f}_n(\eta) = \sum_{k=0}^{K-1} \frac{\hat{P}\{B_k\}}{h_{k+1} - h_k} I_{B_k}(\eta). \quad (2.7)$$

In Eq. (2.7),  $\{h_0, \dots, h_K\}$  are the histogram breakpoints,  $\{B_k = [h_k, h_{k+1})\}$  are the histogram bins,  $\hat{P}\{B_k\}$  is the relative frequency of each bin, i.e.,

$$\hat{P}[B_k] = \frac{1}{Q} \sum_{j=1}^Q I_{B_k}(\eta_j), \quad (2.8)$$

and  $I_A(y)$  is the set indicator function, defined as 1 for  $y \in A$ , and 0 otherwise.

Given the histogram estimate  $\hat{f}_n(\cdot)$ , the next step is to estimate the derivative of  $\ln[\hat{f}_n(\rho_i)]$ . If it is assumed that the actual pdf,  $f_n(\rho_i)$ , is continuous, then the impulses that arise from differentiating Eq. (2.7) do not accurately model  $\frac{d}{d\rho_i} \ln[f_n(\rho_i)]$ . To remedy this dilemma another way of viewing the histogram is utilized. One can think of the process of assigning samples to a bin as a form of quantization. In other words, all  $\rho_i$  in the range  $[h_k, h_{k+1})$  are quantized to  $h_k$ . Then, a three-point numerical approximation of the derivative of  $\ln[f_n(\rho_i)]$  evaluated at  $h_k$  is used, i.e.,

$$\begin{aligned} \frac{\partial}{\partial \rho_i} \ln[\hat{f}_n(\rho_i)] \Big|_{\rho_i=h_k} &\approx \frac{\ln[\hat{f}_n(h_{k+1})] - \ln[\hat{f}_n(h_{k-1})]}{h_{k+1} - h_{k-1}} \\ &\approx \frac{\ln[\hat{P}(B_{k+1})] - \ln[\hat{P}(B_{k-1})]}{h_{k+1} - h_{k-1}} \\ &\quad - \frac{\ln[h_{k+2} - h_{k+1}] - \ln[h_k - h_{k-1}]}{h_{k+1} - h_{k-1}}. \end{aligned} \quad (2.9)$$

If the bins have equal width, Eq. (2.9) reduces to

$$\frac{\partial}{\partial \rho_i} \ln[f_n(\rho_i)] \Big|_{\rho_i=h_k} \approx \frac{\ln[\hat{P}\{B_{k+1}\}] - \ln[\hat{P}\{B_{k-1}\}]}{2\Delta}, \quad (2.10)$$

where  $\Delta$  is the width of a bin. Finally, assuming bins of equal width, the value of the approximation in Eq. (2.10) is extended from  $h_k$  to all  $\rho_i$  in the range  $[h_k, h_{k+1})$ , yielding the histogram implementation of the memoryless LO nonlinearity:

$$\hat{g}_H(\rho_i) = -\frac{1}{2\Delta} \sum_{k=0}^{K-1} [\ln \hat{P}\{B_{k+1}\} - \ln \hat{P}\{B_{k-1}\}] I_{B_k}(\rho_i). \quad (2.11)$$

As a result of the three-point approximation of the derivative, the expression in Eq. (2.11) requires values for  $\hat{P}\{B_{-1}\}$  and  $\hat{P}\{B_K\}$ , which are outside the support of the histogram pdf estimate. Instead, one can use a two-point approximation of the derivative in the first and last histogram bins. This modification is equivalent to defining  $\hat{P}\{B_{-1}\} \triangleq \hat{P}^2\{B_0\}/\hat{P}\{B_1\}$  and  $\hat{P}\{B_K\} \triangleq \hat{P}^2\{B_{K-1}\}/\hat{P}\{B_{K-2}\}$ .

The estimation of a pdf using a histogram usually requires a large number of samples [15]. Thus  $Q$ , the total number of observed samples used to construct the histogram, may be much larger than  $N$ , the number of samples in each signal vector. To obtain the total number of required observed samples, the value of  $Q$  should be chosen such that  $Q = CN$ , where  $C$  is an integer chosen to yield enough samples to construct an accurate histogram. The  $C$  vectors can be stored and all the available samples used to compute the histogram. Detection can then be performed on each data vector using the resulting histogram to compute the approximate nonlinearity of Eq. (2.11).

## 2.2 The Direct FSA Robust LO Detector

Given a few simplifying assumptions, methods can be derived to *directly* approximate the LO nonlinearity of Eq. (2.4). One such method yields the direct FSA robust LO detector [14]. To derive this detector, let  $\{\eta_j\}$  as the set of  $Q$  observed samples of the noise random variable,  $n$ . Furthermore, assume that  $f_n(\eta)$  is even symmetric and has finite support with endpoints given by  $\eta_{max}$  and  $\eta_{min} = -\eta_{max}$ . Then, the resulting FSA implementation of the robust LO nonlinearity has the form [14]

$$\hat{g}_F(\rho_i) = \sum_{k=1}^P b_k \sin(k\omega_0\rho_i) I_{(\eta_{min}, \eta_{max})}(\rho_i), \quad (2.12)$$

where  $T_0 \triangleq (\eta_{max} - \eta_{min})$ ,  $\omega_0 \triangleq 2\pi/T_0$ , and  $p$  is the FSA order. The coefficients  $\mathbf{b} = [b_1 \dots b_p]^T$  are determined by minimizing the mean squared error between  $g(\rho_i)$  and  $\hat{g}_F(\rho_i)$ , written as

$$\begin{aligned} J &= E \{ [g(r) - \hat{g}_F(r)]^2 \} |_{r=n} = \int_{-\infty}^{\infty} [g(\rho) - \hat{g}_F(\rho)]^2 f_n(\rho) d\rho \\ &= \int_{\eta_{min}}^{\eta_{max}} \left[ g(\rho) - \sum_{k=1}^p b_k \sin(k\omega_0\rho) \right]^2 f_n(\rho) d\rho. \end{aligned} \quad (2.13)$$

After some manipulation, it can be shown that the FSA coefficients are given by [14]

$$\mathbf{b} = 2\omega_0 \mathbf{T}^{-1} \mathbf{c}, \quad (2.14)$$

where

$$\mathbf{c} \triangleq [\hat{\Phi}_n(\omega_0) \ 2\hat{\Phi}_n(2\omega_0) \ \dots \ p\hat{\Phi}_n(p\omega_0)]^T, \quad (2.15)$$

and

$$\mathbf{T} \triangleq \begin{bmatrix} 1 - \hat{\Phi}_n(2\omega_0) & \dots & \hat{\Phi}_n[(p-1)\omega_0] \\ & & -\hat{\Phi}_n[(p+1)\omega_0] \\ \hat{\Phi}_n(\omega_0) & \dots & \hat{\Phi}_n[(p-2)\omega_0] \\ -\hat{\Phi}_n(3\omega_0) & \dots & -\hat{\Phi}_n[(p+2)\omega_0] \\ \vdots & & \vdots \\ \hat{\Phi}_n[(p-1)\omega_0] & \dots & 1 - \hat{\Phi}_n(2p\omega_0) \\ -\hat{\Phi}_n[(p+1)\omega_0] & & \end{bmatrix}. \quad (2.16)$$

In Eq. (2.15) and Eq. (2.16),  $\Phi_n(\omega) = E\{\cos(\omega n)\}$  is the *characteristic function* (CF) of  $f_n(\cdot)$ , and  $\hat{\Phi}_n(k\omega_0)$  is an estimate of  $\Phi_n(k\omega_0)$ , given by

$$\hat{\Phi}_n(k\omega_0) = \frac{1}{Q} \sum_{j=1}^Q \cos(k\omega_0\eta_j). \quad (2.17)$$

With a slight modification, the FSA nonlinearity of Eq. (2.12) can be used for the case when  $f_n(\eta)$  has infinite support, as in the case of the Gaussian and Cauchy pdfs. In these instances  $\eta_{max}$  can be chosen as  $\eta_{max} = C \max(|\rho_{max}|, |\rho_{min}|)$ , where  $\rho_{max}$  and  $\rho_{min}$  are the maximum and minimum observations of the received signal, and  $C \geq 1$  is a constant. The result will be a truncated estimate of the actual unbounded LO nonlinearity, and

in most cases will provide a suitable approximation given that the range of observed signal values is bounded.

## Chapter 3

# Enhancement Techniques

The robust LO detector algorithms described in Chapter 2 require observations,  $\{\eta_j\}$ , of the random noise variable,  $n$ . However, in most applications of interest, uncorrupted noise samples are not available at the detector. For low *signal-to-noise ratio* SNR environments, one method for removing this requirement is to use a *small signal assumption*, or an equivalent *high J/S assumption*. Thus, typical robust LO detectors use the received signal samples to estimate the noise pdf, from which the required nonlinearity is formed. However, previous work by Ucci et al. [12], and the additional results provided in the next chapter, suggest that the large interference assumption that the noise samples can be approximated by the received signal samples (or that the noise pdf can be approximated by the received signal pdf) is not always sufficient, even in large *J/S* environments. Thus, this chapter presents three potential robust detector enhancement techniques for improving the effectiveness of the various detector algorithms for the case of binary detection of real signals. As will be seen, these methods focus on obtaining an estimate of the noise pdf or *characteristic function* (CF) from an initial estimate of the received signal pdf or CF, along with knowledge of the information signal. Supporting examples are provided where applicable.

### 3.1 The Least Squares Method

The *least squares* (LS) enhancement technique focuses on obtaining an estimate of the noise pdf from an initial estimate of the received signal pdf,

along with knowledge of the information signal. Since the various pdfs will ultimately be processed in a computer (or some digital processor), the LS technique operates on “discrete” versions of the original continuous pdfs, possibly obtained by sampling at regular intervals. This assumption allows the use of well-known *digital signal processing* (DSP) techniques. Specifically, let  $f_{\mathbf{r}}[\mathbf{k}] = f_{\mathbf{r}}[k_1, \dots, k_N] = f_{\mathbf{r}}(k_1 T_1, \dots, k_N T_N)$  denote the “discrete” version of the  $N$ -dimensional received signal pdf, where  $N$  is the number of signal samples in a given symbol period and  $\{T_j\}$  are the “sampling” periods for each dimension. Similarly, let  $f_{\mathbf{s}}[\mathbf{k}]$  and  $f_{\mathbf{n}}[\mathbf{k}]$  be the “discrete” versions of the information signal and noise pdfs, respectively. Then, assuming that the information signal and noise are independent,

$$f_{\mathbf{r}}[\mathbf{k}] = f_{\mathbf{s}}[\mathbf{k}] * f_{\mathbf{n}}[\mathbf{k}]. \quad (3.1)$$

For the LS enhancement technique, the goal is to find a finite length, stable inverse filter, denoted as  $h[\mathbf{k}]$ , such that

$$h[\mathbf{k}] * f_{\mathbf{r}}[\mathbf{k}] \approx f_{\mathbf{n}}[\mathbf{k}], \quad (3.2)$$

or equivalently,

$$h[\mathbf{k}] * f_{\mathbf{s}}[\mathbf{k}] \approx \delta[\mathbf{k}], \quad (3.3)$$

where  $\delta[\mathbf{k}]$  is the multivariate discrete impulse function. To find such a filter, consider the least squares filtering problem shown in Fig. 3.1. In the case at hand the input signal is  $f_{\mathbf{s}}[\mathbf{k}]$ , and the desired output signal is  $d[\mathbf{k}] = \delta[\mathbf{k}]$ . The error at the output of the least squares filter is

$$e[\mathbf{k}] = d[\mathbf{k}] - \sum_{\mathbf{i}} h[\mathbf{i}] f_{\mathbf{s}}[\mathbf{k} - \mathbf{i}] \quad (3.4)$$

where the range of summation depends on the length of the filter. The solution for  $h$  is found by minimizing the squared error

$$J = \sum_{\mathbf{k}} e^2[\mathbf{k}], \quad (3.5)$$

yielding the normal equations

$$\sum_{\mathbf{i}} h[\mathbf{i}] r[\mathbf{j} - \mathbf{i}] = g[\mathbf{j}], \quad (3.6)$$

where  $r[\mathbf{m}] \triangleq \sum_{\mathbf{k}} f_s[\mathbf{k}] f_s[\mathbf{k} + \mathbf{m}]$  is the autocorrelation sequence of  $f_s[\mathbf{k}]$ ,  $g[\mathbf{j}] \triangleq \sum_{\mathbf{k}} d[\mathbf{k}] f_s[\mathbf{k} - \mathbf{j}]$ , and  $\mathbf{j}$  varies over the same range as  $\mathbf{i}$ . Since  $d[\mathbf{k}] = \delta[\mathbf{k}]$ ,  $g[\mathbf{j}]$  becomes

$$g[\mathbf{j}] = f_s[-\mathbf{j}], \quad (3.7)$$

resulting in the normal equations for the pdf deconvolution problem:

$$\sum_{\mathbf{i}} h[\mathbf{i}] r[\mathbf{j} - \mathbf{i}] = f_s[-\mathbf{j}]. \quad (3.8)$$

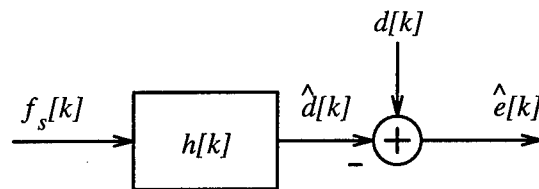


Figure 3.1: A typical least squares filtering problem.

### 3.1.1 The LS Enhanced BPSK LO Detector for Independent Noise

This research effort focuses on the straightforward problem of detecting a BPSK signal in iid additive noise. Let the “discrete” amplitude of the BPSK signal be a constant value,  $a$ . Since the noise is iid, the detector algorithms are based on the marginal pdf of the noise. The corresponding marginal pdf of the information signal has the form

$$f_s[k] = \frac{1}{2} (\delta[k + a] + \delta[k - a]). \quad (3.9)$$

For a two-sided filter having total length  $2L - 1$ , the LS filter,  $h$ , is the solution to the normal equations in Eq. (3.8), which in this case are

$$\sum_{i=-(L-1)}^{L-1} h[i] r[j - i] = g[j], \quad (3.10)$$

where  $r[m] = \sum_k f_s[k]f_s[k+m]$ , and  $g[j] = \sum_k d[k]f_s[k-j] = f_s[-j]$ . From Eq. (3.9), it can be shown that  $r[m]$  is given by

$$r[m] = \frac{1}{4}\delta[m+2a] + \frac{1}{2}\delta[m] + \frac{1}{4}\delta[m-2a]. \quad (3.11)$$

Writing Eq. (3.10) in matrix form,  $h$  is found as the solution to the equation

$$\mathbf{R}h = \mathbf{g} \quad (3.12)$$

where

$$\mathbf{R} = \begin{bmatrix} 1/2 & 0 & \overbrace{\dots}^{2a-3} & 0 & 1/4 & 0 & \overbrace{\dots}^{2(L-a)-4} & 0 \\ 0 & \ddots & \ddots & & \ddots & \ddots & \ddots & \vdots \\ \vdots & \ddots & \ddots & \ddots & & \ddots & \ddots & 0 \\ 0 & & \ddots & \ddots & \ddots & & \ddots & 1/4 \\ 1/4 & \ddots & & \ddots & \ddots & \ddots & & 0 \\ 0 & \ddots & \ddots & & \ddots & \ddots & \ddots & \vdots \\ \vdots & \ddots & \ddots & \ddots & & \ddots & \ddots & 0 \\ 0 & \dots & 0 & 1/4 & 0 & \dots & 0 & 1/2 \end{bmatrix}, \quad (3.13)$$

$$\mathbf{h} = \begin{bmatrix} h(-L+1) \\ h(-L+2) \\ \vdots \\ \vdots \\ \vdots \\ \vdots \\ h(L-2) \\ h(L-1) \end{bmatrix}, \quad (3.14)$$



and

$$\mathbf{g} = \begin{bmatrix} 0 \\ \vdots \\ 0 \\ 1/2 \\ 0 \\ 1/2 \\ 0 \\ \vdots \\ 0 \end{bmatrix} \quad (3.15)$$

### 3.1.2 Sample Operation

A simulation was developed using the software package Matlab™ by The MathWorks, Inc. to examine the LS enhanced robust LO detector in a *direct sequence (DS) spread spectrum (SS)* system. The resulting simulation algorithm can be divided into the following steps:

1. The transmitted and noise signals are constructed, then added together to form the received signal.
2. The received signal is soft-limited or noise-blanked to eliminate the large interference amplitudes, facilitating histogram construction.
3. A  $K$ -bin histogram of the modified received signal is constructed, with the number of bins specified by the user. The number of bins must be odd so that the histogram is centered about zero.
4. The amplitude of the BPSK signal,  $a$ , is assigned to a histogram bin. This bin index,  $k_a$ , determines the filter extension factor (see Step 6).
5. The LS inverse filter,  $h_1$ , is determined for the case when  $k_a = 1$ .
6. This filter is *extended* by inserting  $(k_a - 1)$  zeros between each of the original filter coefficients. The resulting filter is the LS inverse filter,

$h_a$ , for the general case where the transmitted signal amplitude falls into the  $k_a^{th}$  bin.<sup>1</sup>

7. The received signal histogram is convolved with  $h_a$  to yield the estimate of the noise pdf,  $\hat{f}_n$ . The estimate is truncated to length  $K - 2k_a$ .
8. The LO nonlinearity,  $\hat{g}$ , is estimated from  $\hat{f}_n$ .
9. Finally,  $\hat{g}$  is used to decode the received data.

An example of the operation of the LS enhanced detector in Cauchy noise is shown in Fig. 3.2 to Fig. 3.8. Figure 3.2 illustrates a received signal histogram for the case when the number of bins is  $K = 99$  and  $E_c/\sigma = 8 dB$ , where  $E_c/\sigma$  is the ratio of the chip energy to the Cauchy scale parameter. Two noise histograms, one estimated using actual noise samples, and the other an LS enhanced estimate using the received signal samples, are given in Fig. 3.3 and Fig. 3.4, respectively. As can be seen, the deconvolution operation yields a good approximation in the center of the pdf, but produces artifacts in the tails. Next, the LO nonlinearities constructed from these two noise histograms are shown in Fig. 3.5 to Fig. 3.7. The two nonlinearities are approximately equal in the region centered about zero, but the LS enhanced version has larger error in the tail regions, a result of the tail artifacts in the pdf estimate. However, if the majority of received signal samples lie in the region where the two approximations are similar (see Fig. 3.2), i.e., if the bin index  $k_a$  is an accurate representation of the signal amplitude,  $a$ , thus causing  $h$  to be a good model of the true inverse filter, then these tail errors cause only minimal performance degradation in many situations (see Section 4.1.1). Finally, the LS deconvolution filter derived using the method discussed in Section 3.1.1 and Section 3.1.2, and used to implement the LS

---

<sup>1</sup>This reduced computation method for determining  $h_a$  can be understood by examining the following interpolation problem. Consider the case when the BPSK amplitude is such that  $k_a = 1$ . Using Eq. (3.9), let  $\hat{f}_s[k] = \frac{1}{2}(\delta[k+1] + \delta[k-1]) \triangleq f_1[k]$ . Let  $h_1$  be the LS inverse filter for  $f_1[k]$ , and the resulting *mean squared error* (MSE) be  $J_1$ . Next, consider the case when the BPSK amplitude is such that it falls into the  $k_a^{th}$  bin, and let  $\hat{f}_s[k] = \frac{1}{2}(\delta[k+k_a] + \delta[k-k_a]) \triangleq f_a[k]$ . The function  $f_a[k]$  can be constructed from  $f_1[k]$  by interpolating  $f_1[k]$  by a factor of  $k_a$ , i.e., inserting  $(k_a - 1)$  zeros between each sample of  $f_1[k]$ . Thus, if the LS inverse filter for  $f_a[k]$ , denoted as  $h_a$ , is constructed by interpolating  $h_1$  by a factor of  $k_a$ , the resulting MSE is  $J_a = J_1$ , the minimum.

technique for this example, is provided in Fig. 3.8. For a more detailed performance analysis of the LS enhancement method, see Chapter 4 of this report.

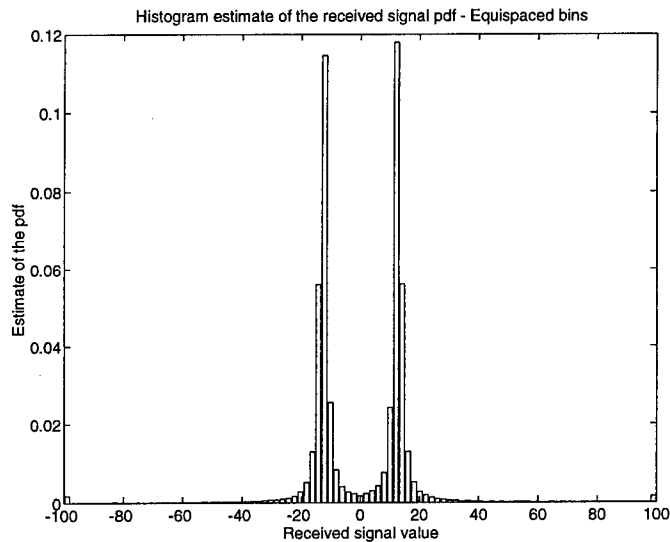


Figure 3.2: Histogram estimate of the received signal pdf,  $K = 99$ ,  $T = 200$ ,  $E_c/\sigma = 8 \text{ dB}$ .

## 3.2 The Characteristic Function Method

The CF enhancement technique also focuses on obtaining an estimate of the noise pdf from an initial estimate of the received signal pdf. Additionally, an estimate of the CF of the noise can be obtained from an initial estimate of the CF of the received signal, which can be used to enhance direct LO implementation methods, such as the direct FSA algorithm. The CF method is developed as follows. As in Section 3.1, let  $f_{\mathbf{r}}[\mathbf{k}]$ ,  $f_{\mathbf{s}}[\mathbf{k}]$  and  $f_{\mathbf{n}}[\mathbf{k}]$  denote the discrete versions of the received signal, information signal and noise pdfs, respectively. Then, as before,  $f_{\mathbf{r}}[\mathbf{k}]$  is related to  $f_{\mathbf{s}}[\mathbf{k}]$  and  $f_{\mathbf{n}}[\mathbf{k}]$  by the convolution operation described by Eq. (3.1).

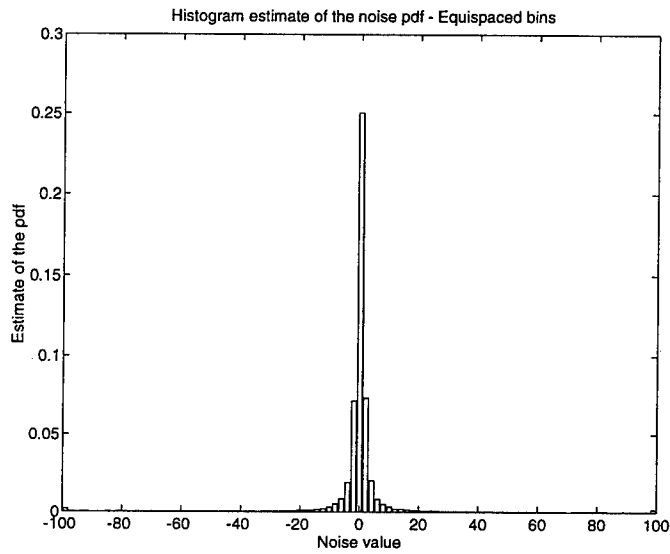


Figure 3.3: Histogram estimate of the noise pdf,  $K = 99$ ,  $T = 200$ ,  $E_c/\sigma = 8 \text{ dB}$ .

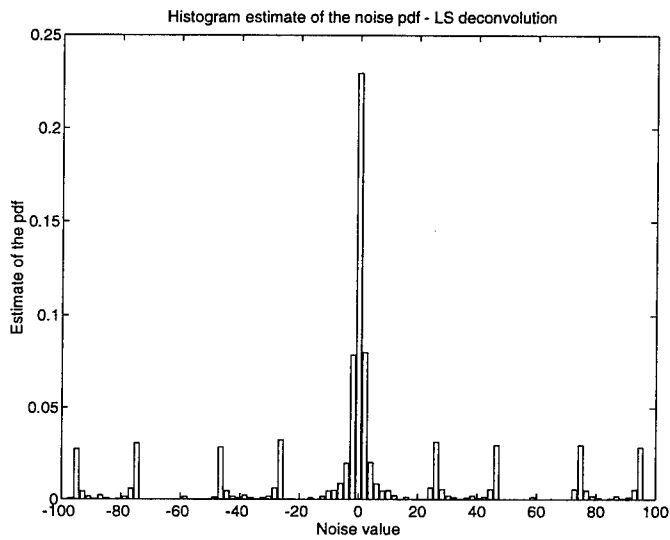


Figure 3.4: LS enhanced histogram estimate of the noise signal pdf,  $K = 99$ ,  $T = 200$ ,  $E_c/\sigma = 8 \text{ dB}$ ,  $L = 50$ .

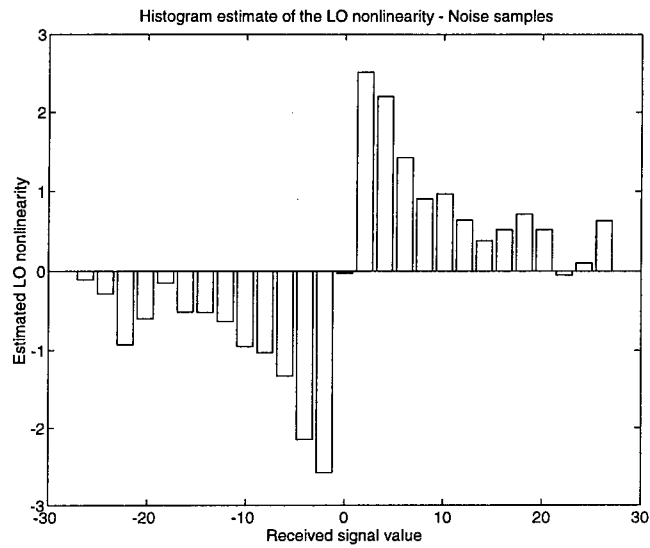


Figure 3.5: Histogram estimate of the LO nonlinearity using noise samples,  $K = 99$ ,  $T = 200$ ,  $E_c/\sigma = 8 \text{ dB}$ .

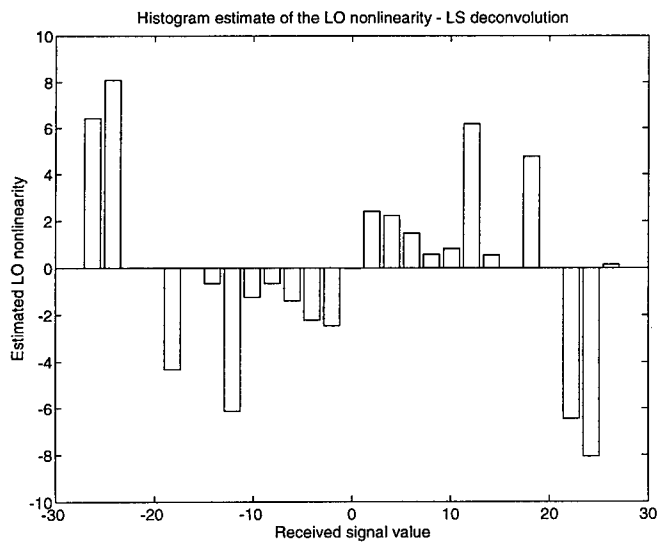


Figure 3.6: LS enhanced histogram estimate of the LO nonlinearity,  $K = 99$ ,  $T = 200$ ,  $E_c/\sigma = 8 \text{ dB}$ ,  $L = 50$ .

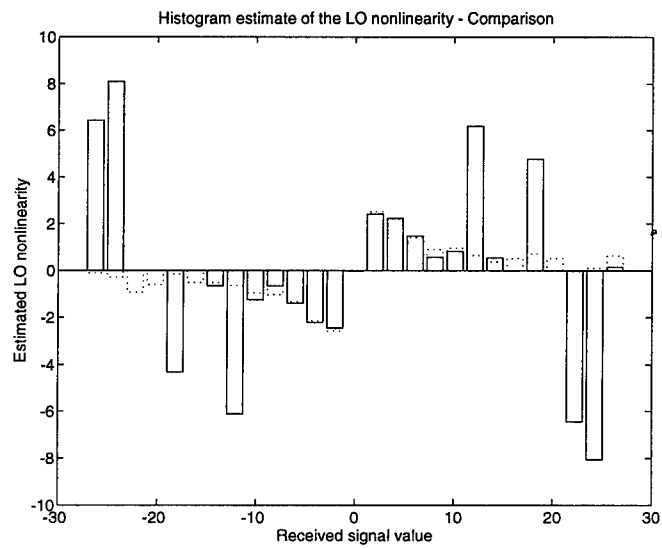


Figure 3.7: Comparison of the two LO nonlinearity estimates,  $K = 99$ ,  $T = 200$ ,  $E_c/\sigma = 8 \text{ dB}$ ,  $L = 50$ . Legend: — LS enhancement, ... Estimate using noise samples

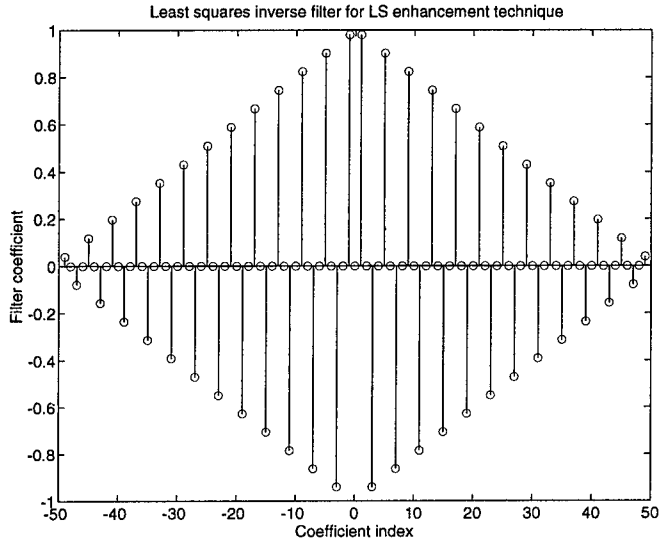


Figure 3.8: The LS deconvolution filter,  $K = 99$ ,  $T = 200$ ,  $E_c/\sigma = 8 \text{ dB}$ ,  $L = 50$ .

Recall that the CF of  $f_{\mathbf{r}}[\mathbf{k}]$ , denoted as  $\Phi_{\mathbf{r}}(\omega)$ , is given by [16]

$$\Phi_{\mathbf{r}}(\omega) = F_{\mathbf{r}}(e^{-j\omega}) = \sum_{\mathbf{k}} f_{\mathbf{r}}[\mathbf{k}] \cdot e^{j(\omega^T \mathbf{k})} \quad (3.16)$$

where  $F_{\mathbf{r}}(e^{j\omega})$  is the  $N$ -dimensional *Fourier transform* (FT) of  $f_{\mathbf{r}}[\mathbf{k}]$ . Substituting Eq. (3.1) into Eq. (3.16),  $F_{\mathbf{r}}(e^{j\omega})$  may be written as [16]

$$F_{\mathbf{r}}(e^{j\omega}) = F_s(e^{j\omega})F_n(e^{j\omega}) \quad (3.17)$$

where  $F_s(e^{j\omega})$  is the FT of  $f_s[\mathbf{k}]$ , and  $F_n(e^{j\omega})$  is the FT of  $f_n[\mathbf{k}]$ . As can be seen, given knowledge of  $F_s(e^{j\omega})$ , an estimate of  $F_{\mathbf{r}}(e^{j\omega})$ , and using Eq. (3.17), the noise FT may be estimated as

$$\hat{F}_n(e^{j\omega}) = \frac{\hat{F}_{\mathbf{r}}(e^{j\omega})}{F_s(e^{j\omega})}. \quad (3.18)$$

Thus, the goal of the CF enhancement technique is to approximate the CF (or FT) of the noise pdf, and in the case of indirect LO detector implementation, invert the result to obtain an accurate estimate of the pdf.

### 3.2.1 The CF Enhanced BPSK LO Detector for Independent Noise

For the case of a BPSK system in iid noise with information signal amplitude  $a$ , the information signal pdf is given by Eq. (3.9). Using Eq. (3.16), it can be shown that the FT of the transmitted signal pdf is

$$F_s(e^{j\omega}) = \cos(\omega a). \quad (3.19)$$

Thus, given an estimate of the FT of the received signal pdf, the resulting expression for  $\hat{F}_n(e^{j\omega})$  is

$$\hat{F}_n(e^{j\omega}) = \frac{\hat{F}_r(e^{j\omega})}{\cos(\omega a)}. \quad (3.20)$$

Note that it is possible that  $|\hat{F}_n(e^{j\omega})| \rightarrow \infty$  when  $\omega a$  equals  $(2i + 1)\pi/2$  for any integer  $i$ . Therefore, this method may prove unstable in practice, and further modifications may be required.

### 3.2.2 Sample Operation

A simulation of the CF enhanced histogram LO detector for BPSK signals in iid additive noise was developed using the Matlab<sup>TM</sup> software package. The simulation algorithm can be divided into the following steps:

1. The transmitted and noise signals are constructed, then added together to form the received signal.
2. The received signal is soft-limited or noise-blanked to eliminate the large interference amplitudes, facilitating histogram construction.
3. A  $K$ -bin histogram of the modified received signal is constructed, with the number of bins specified by the user. The number of bins must be odd so that the histogram is centered about zero.
4. The amplitude of the BPSK signal,  $a$ , is assigned to a histogram bin,  $k_a$ .
5. The *discrete FT* (DFT) of the received signal histogram is computed.



6. An estimate of the DFT of the noise histogram is constructed using the expression in Eq. (3.20), with  $a$  replaced by  $k_a\Delta$ , where  $\Delta$  is the bin width of the received signal histogram.
7. The DFT of the noise histogram is inverted to yield an estimate of the noise pdf,  $\hat{f}_n$ . The estimate is truncated to length  $K - 2k_a$ .
8. The LO nonlinearity,  $\hat{g}$ , is estimated from  $\hat{f}_n$ .
9. Finally,  $\hat{g}$  is used to decode the received data.

Figure 3.9 through Fig. 3.15 illustrate a sample operation of the CF enhanced histogram robust LO detector in Cauchy noise. In particular, the resulting estimates of the noise CF, noise pdf, and LO nonlinearity are provided for the case of  $K = 33$ ,  $T = 50$ , and  $E_c/\sigma = -1$  dB. Figure 3.9 depicts a typical histogram estimate of the received signal pdf for this scenario. Two noise histograms, one estimated using uncorrupted noise samples, and the other estimated using the received signal samples in conjunction with the CF technique, are depicted in Fig. 3.10 and Fig. 3.11. Similar to the LS enhancement case, the CF technique provides a good estimate in the center region of the noise pdf, but yields artifacts in the tail regions. The robust LO nonlinearities corresponding to these pdf estimates are shown in Fig. 3.12 to Fig. 3.14. By comparing the two nonlinearities, as in Fig. 3.14, it is readily evident that the CF technique produces a nonlinearity that is similar to the desired one in the region about zero, but has artifacts in the tail regions resulting from the artifacts in the noise pdf estimate. For completeness, Fig. 3.15 shows the DFT of the noise histogram estimated using the CF technique. In this figure, the solid line represents the estimated DFT, and the dotted line represents the theoretical DFT obtained given knowledge of the mathematical expression for the noise pdf. As can be seen, the CF technique yields a relatively good estimate of the true DFT, with the largest error associated with those bins nearest the BPSK signal amplitude. See Chapter 4 for further investigation of the performance of the CF enhancement technique.

### 3.3 The Preamble Method

One limitation of the LS enhancement technique is that it yields an estimate of the noise pdf, and not estimates of the actual noise samples. Thus, this

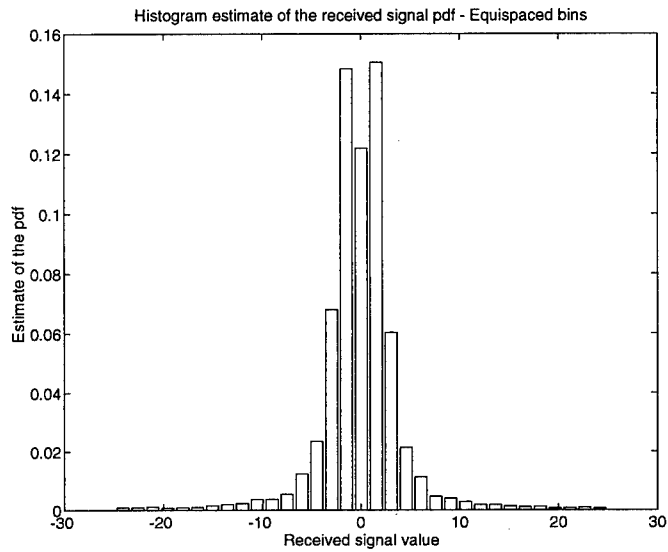


Figure 3.9: Histogram estimate of the received signal pdf,  $K = 33$ ,  $T = 50$ ,  $E_c/\sigma = -1$  dB.

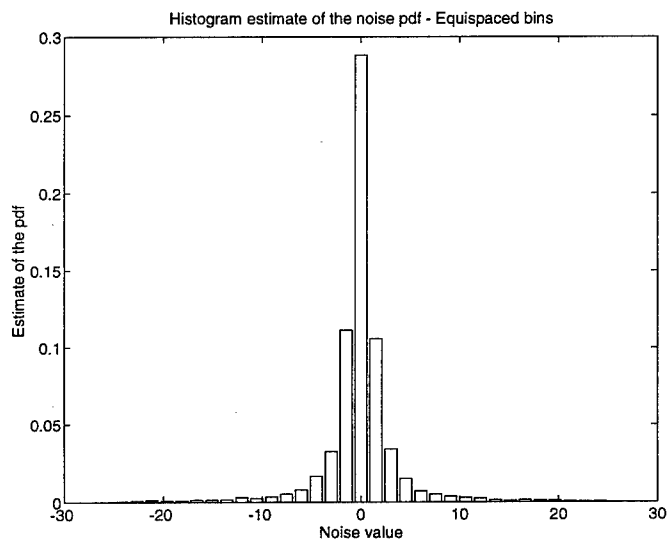


Figure 3.10: Histogram estimate of the noise pdf,  $K = 33$ ,  $T = 50$ ,  $E_c/\sigma = -1$  dB.

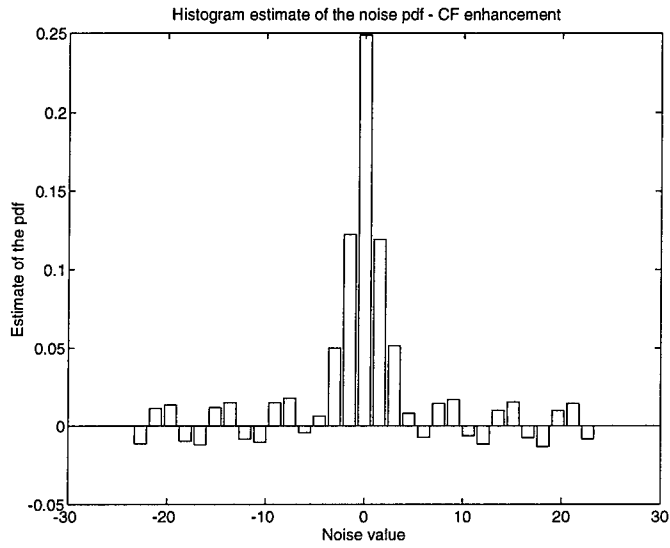


Figure 3.11: CF enhanced histogram estimate of the noise signal pdf,  $K = 33$ ,  $T = 50$ ,  $E_c/\sigma = -1$  dB.

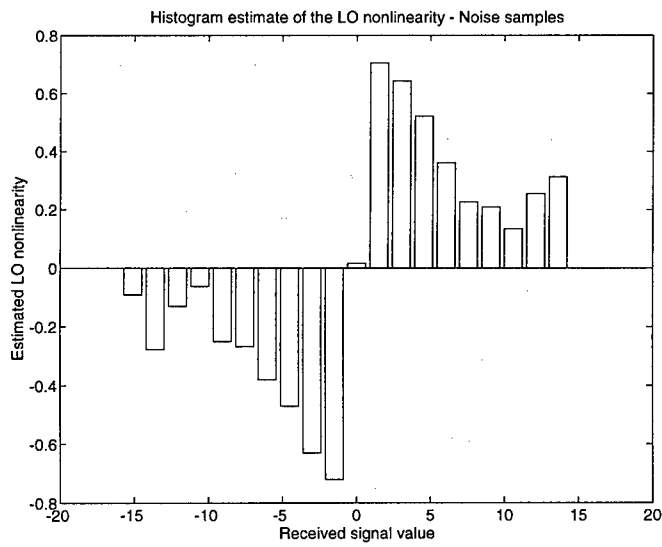


Figure 3.12: Histogram estimate of the LO nonlinearity using noise samples,  $K = 33$ ,  $T = 50$ ,  $E_c/\sigma = -1$  dB.

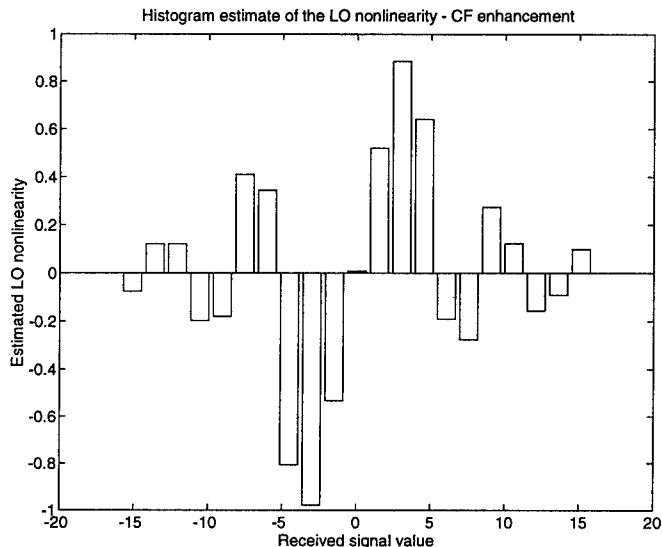


Figure 3.13: CF enhanced histogram estimate of the LO nonlinearity,  $K = 33$ ,  $T = 50$ ,  $E_c/\sigma = -1$  dB.

method is primarily suited to indirect methods of robust LO detector implementation, and is not readily applicable to direct implementation methods. Also, the CF enhancement technique, while applicable to both indirect and direct methods (e.g., the direct FSA method [14]), suffers from limitations associated with estimating the information signal's amplitude and the CF of the received signal pdf (see Chapter 4 of this report).

This section presents the preamble enhancement technique, a method that may be applied to direct *and* indirect LO detector implementation algorithms. In particular, this method yields an estimate of the CF of the noise pdf that does not require intermediate estimates of the information signal amplitude and CF of the received signal pdf. Thus, the preamble technique does not possess many of the limitations inherent to the CF and LS methods.

To begin, consider a known training sequence of the form

$$\mathbf{s} = [s_1, s_2, \dots, s_Q]^T = [1, -1, 1, -1, \dots]. \quad (3.21)$$

Let the received signal at the input to the detector be given by

$$r_i = \theta s_i + n_i, \quad i = 1, \dots, Q, \quad (3.22)$$

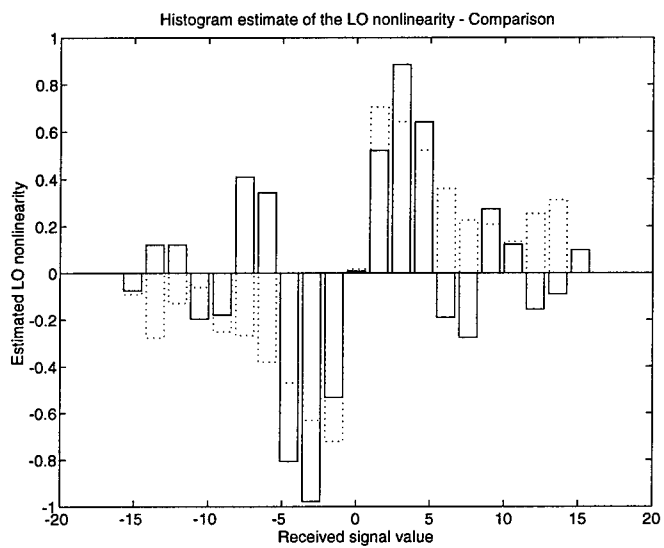


Figure 3.14: Comparison of the two LO nonlinearity estimates,  $K = 33$ ,  $T = 50$ ,  $E_c/\sigma = -1 \text{ dB}$ . Legend: — CF enhancement, .... Estimate using noise samples

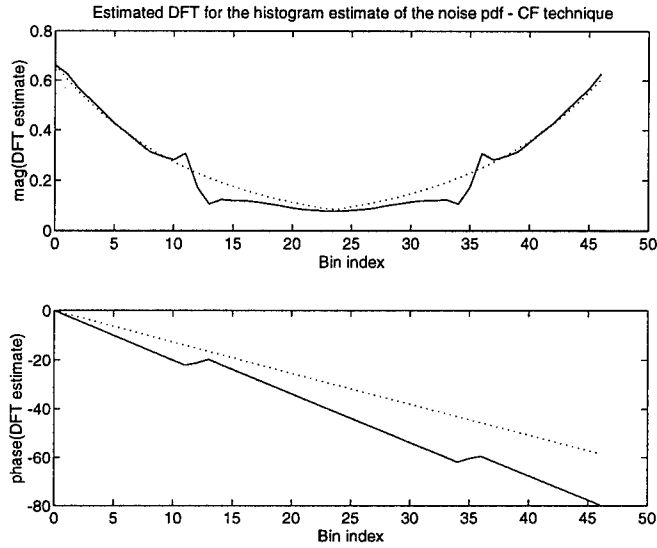


Figure 3.15: Estimate of the histogram DFT using the CF technique,  $K = 33$ ,  $T = 50$ ,  $E_c/\sigma = -1$  dB. Legend: — CF enhancement, .... Theoretical

where  $n_i$  represents the iid noise samples and  $\theta$  is the unknown signal amplitude. Given that the  $s_i$  are known (during training), one would like to subtract the information signal component from Eq. (3.22) to yield an uncorrupted noise sample. However, this operation cannot be performed directly since in many cases the amplitude of the information signal is unknown at the detector.

To derive the preamble technique, assume the following: 1)  $\theta$  is relatively constant over an extended period of time (slow fading); 2) the noise samples are iid with an even symmetric pdf,  $f_n(x)$ ; and 3) perfect synchronization is achieved prior to training. Then, given these assumptions, consider the sequences  $\mathbf{v} = [v_1, v_2, \dots, v_{Q_1}]$  and  $\mathbf{w} = [w_1, w_2, \dots, w_{Q_2}]$ , where

$$v_i = (s_{2i-1}r_{2i-1} - s_{2i}r_{2i}) = n_{2i-1} + n_{2i}, \quad i = 1, \dots, Q_1, \quad (3.23)$$

and

$$\begin{aligned} w_i &= (-1)^{i-1} [(s_{3i-2}r_{3i-2} - s_{3i-1}r_{3i-1}) - (s_{3i-1}r_{3i-1} - s_{3i}r_{3i})] \\ &= n_{3i-2} + 2n_{3i-1} + n_{3i}, \quad i = 1, \dots, Q_2. \end{aligned} \quad (3.24)$$

Since each  $v_i$  is a function of two adjacent samples,  $Q_1 = Q/2$ . Similarly, since each  $w_i$  is a function of three adjacent samples,  $Q_2 = Q/3$ . Thus, for both relationships to be valid,  $Q$  must be divisible by 6.

Continuing, it can be shown that the pdfs of  $v_i$  and  $w_i$  are [16]

$$f_v(x) = f_n(x) * f_n(x) \quad (3.25)$$

and

$$f_w(x) = \frac{1}{2} f_n(x) * f_n(x) * f_n(x/2). \quad (3.26)$$

Furthermore, the CFs of  $f_v(x)$  and  $f_w(x)$  are [16]

$$\Phi_v(\omega) = \Phi_n^2(\omega) \quad (3.27)$$

and

$$\Phi_w(\omega) = \Phi_n^2(\omega) \Phi_n(2\omega) = \Phi_v(\omega) \Phi_n(2\omega). \quad (3.28)$$

Since  $f_n(x)$  is even symmetric, both  $f_v(x)$  and  $f_w(x)$  are even symmetric. Thus,  $\Phi_n(\omega)$ ,  $\Phi_v(\omega)$ , and  $\Phi_w(\omega)$  can also be written as

$$\Phi_n(\omega) = E\{\cos(\omega n_i)\} \quad (3.29)$$

$$\Phi_v(\omega) = E\{\cos(\omega v_i)\} \quad (3.30)$$

$$\Phi_w(\omega) = E\{\cos(\omega w_i)\}. \quad (3.31)$$

Given the samples  $\{v_i\}$  and  $\{w_i\}$ , and the relationships in Eq. (3.30) and Eq. (3.31), one technique for estimating  $\Phi_v(\omega)$  and  $\Phi_w(\omega)$  is through the following expressions:

$$\hat{\Phi}_v(\omega) = \frac{1}{Q_1} \sum_{i=1}^{Q_1} \cos(\omega v_i) \quad (3.32)$$

$$\hat{\Phi}_w(\omega) = \frac{1}{Q_2} \sum_{i=1}^{Q_2} \cos(\omega w_i). \quad (3.33)$$

Then, using Eq. (3.28), and given the estimates  $\hat{\Phi}_v(\omega)$  and  $\hat{\Phi}_w(\omega)$  provided by Eq. (3.32) and Eq. (3.33),  $\Phi_n(\omega)$  can be estimated as

$$\hat{\Phi}_n(\omega) = \frac{\hat{\Phi}_w(\omega/2)}{\hat{\Phi}_v(\omega/2)} = \frac{Q_1 \sum_{i=1}^{Q_2} \cos(\omega w_i/2)}{Q_2 \sum_{i=1}^{Q_1} \cos(\omega v_i/2)}. \quad (3.34)$$

Finally, Eq. (3.34) can be used to implement the robust LO detector directly, e.g, through the direct FSA method [14]. Equation (3.34) can also be inverted to yield a pdf estimate, from which the robust LO detector can be implemented using one of the many indirect techniques.

### 3.3.1 The Preamble Method and the FSA LO Detector

After comparing Eq. (3.34) to Eq. (2.17), it is readily seen that the preamble enhancement method can be directly applied to the FSA LO detector described in Section 2.2. In particular, the CF estimate of Eq. (2.17) is replaced with the estimate in Eq. (3.34), i.e.,

$$\hat{\Phi}_n(k\omega_0) = \frac{Q_1 \sum_{i=1}^{Q_2} \cos(k\omega_0 w_i/2)}{Q_2 \sum_{i=1}^{Q_1} \cos(k\omega_0 v_i/2)}. \quad (3.35)$$

Then, substituting Eq. (3.35) in Eq. (2.15) and Eq. (2.16), the FSA coefficients are computed as before using the defining expression in Eq. (2.14),

$$\mathbf{b} = 2\omega_0 \mathbf{T}^{-1} \mathbf{c}. \quad (3.36)$$

A sample operation of the preamble enhanced FSA LO detector is provided in Fig. 3.16 through Fig. 3.19 for the case of Cauchy noise and system parameters  $p = 10$ ,  $T = 50$ ,  $Q = 20,000$ , and  $E_c/\sigma = 0 \text{ dB}$ . The desired FSA LO nonlinearity, estimated using uncorrupted noise samples, is shown in Fig. 3.16. Figure 3.17 illustrates the FSA LO nonlinearity estimated using the observed received signal samples. As can be seen from the figure, there is an undesired inflection of the nonlinearity in the region centered about the origin. However, by using the preamble technique, a close approximation of the desired LO nonlinearity can be obtained, as suggested by the FSA LO nonlinearity of Fig. 3.18 constructed using the CF estimates in Fig. 3.19. Note that in implementing the FSA LO nonlinearity using the preamble technique,  $Q = 60,000$  samples were used so that  $Q_2$ , the minimum number of samples forming a CF estimate in Eq. (3.34), had the value  $Q_2 = 20,000$ . Figure 3.19 also illustrates an interesting characteristic of the CF estimator, namely, that for the case of Cauchy noise, the approximation error increases as the frequency,  $k\omega_0$ , increases. This property, as well as the development of a metric for gauging the expected CF estimation error, are the subject of Section 3.3.3. See Chapter 4 for a more detailed analysis of the preamble technique for FSA LO detection.



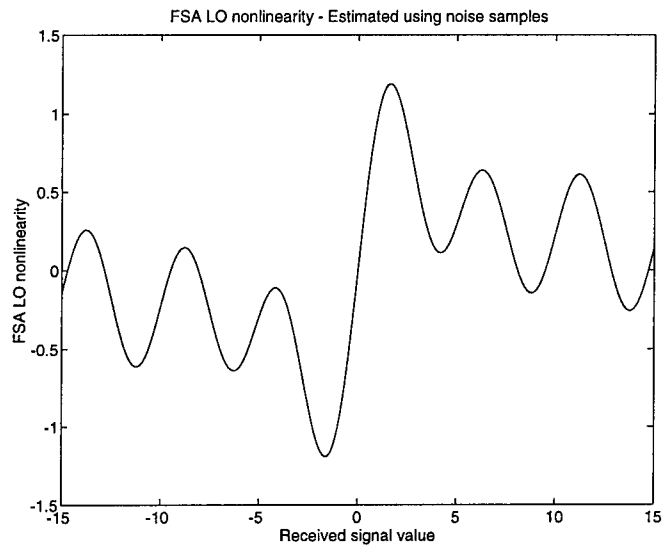


Figure 3.16: FSA LO nonlinearity estimated using noise samples,  $p = 10$ ,  $T = 50$ ,  $Q = 20,000$ ,  $E_c/\sigma = 0 \text{ dB}$ .

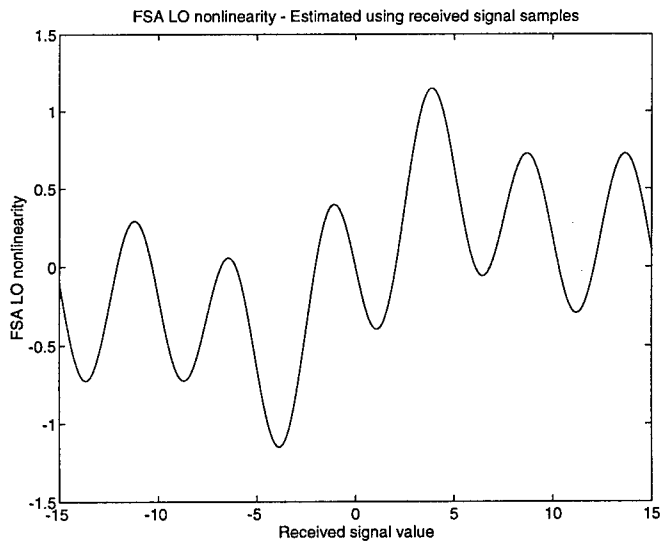


Figure 3.17: FSA LO nonlinearity estimated using received signal samples,  $p = 10$ ,  $T = 50$ ,  $Q = 20,000$ ,  $E_c/\sigma = 0 \text{ dB}$ .

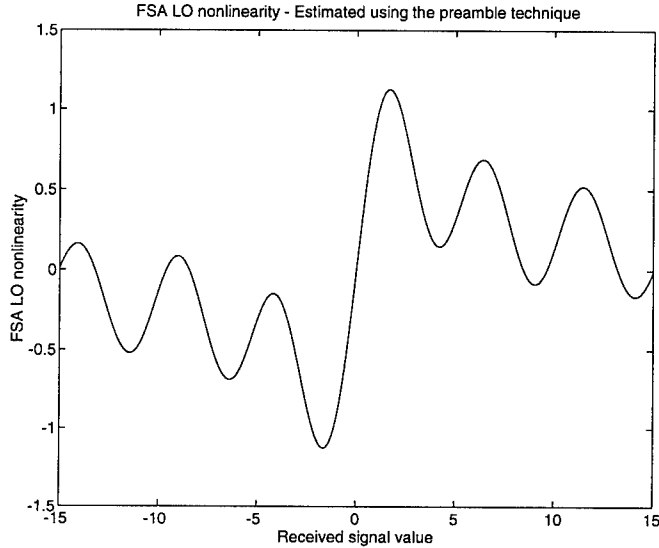


Figure 3.18: FSA LO nonlinearity estimated using the preamble technique,  $p = 10$ ,  $T = 50$ ,  $Q_2 = 20,000$ ,  $E_c/\sigma = 0$  dB.

### 3.3.2 The Preamble Method and the Histogram LO Detector

Contrary to the case of the FSA LO detector, additional development is required before the preamble method can be applied to histogram LO detection. Recall that the preamble method can be used to obtain an estimate of the noise pdf,  $f_n(\eta)$ , by inverting the CF estimate given by Eq. (3.34). However, in the case of histogram LO detection, a histogram estimate of the form

$$\hat{f}_n(\eta) = \sum_{k=0}^{K-1} l_k I_{B_k}(\eta) \quad (3.37)$$

is desired, where  $l_k$  is the value of the histogram in the bin  $B_k$ . For example, the histogram estimator described in Section 2.1 has levels

$$l_k = \frac{\hat{P}\{B_k\}}{h_{k+1} - h_k}, \quad (3.38)$$

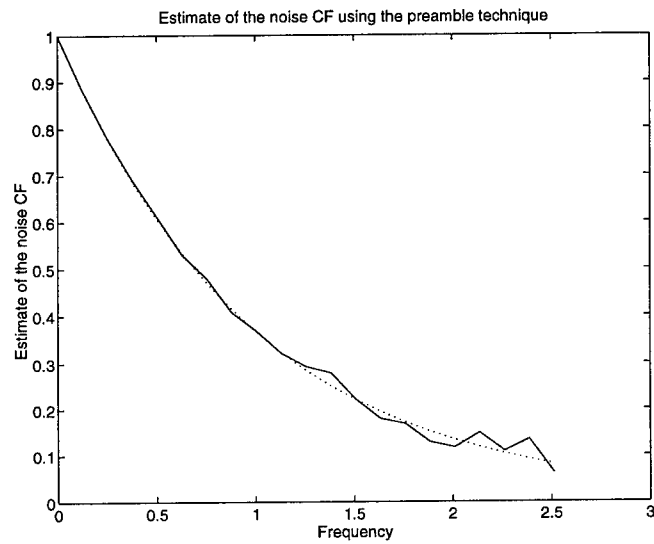


Figure 3.19: Estimate of the noise CF using the preamble technique,  $p = 10$ ,  $T = 50$ ,  $Q = 60,000$  ( $Q_2 = 20,000$ ),  $E_c/\sigma = 0 \text{ dB}$ . Legend: — Preamble technique, .... Theoretical

where  $\hat{P}\{B_k\}$  is the relative frequency of bin  $B_k$ , given by Eq. (2.8), and  $\{h_k\}$  are the bin breakpoints. Once the histogram pdf estimate of Eq. (3.37) is obtained, the corresponding histogram LO nonlinearity can be computed using a method similar to the development of Eq. (2.9) and Eq. (2.10) in Section 2.1.

Examining the histogram levels of Eq. (3.38) in more detail for the case of equal bin width,  $\Delta$ , and for  $f_n(\eta)$  even symmetric, it is evident that, on average,  $\hat{P}\{B_k\}$  approaches  $P\{B_k\}$ , where

$$P\{B_k\} = \int_{h_k}^{h_{k+1}} f_n(\eta) d\eta. \quad (3.39)$$

Thus, the average histogram level,  $\bar{l}_k$ , is

$$\bar{l}_k = \frac{1}{\Delta} \int_{h_k}^{h_{k+1}} f_n(\eta) d\eta, \quad (3.40)$$

which is the mean value of  $f_n(\eta)$  on the interval  $[h_k, h_{k+1})$  [17]. If it is assumed that  $\Delta$  is sufficiently small that, for most cases,  $f_n(\eta)$  is either relatively constant, or monotonically increasing or decreasing in the interval  $[h_k, h_{k+1})$ , then  $\bar{l}_k$  can be approximated as

$$\bar{l}_k \approx f_n \left( \left( k - \frac{K-1}{2} \right) \Delta \right) = f_n \left[ k - \frac{K-1}{2} \right], \quad (3.41)$$

for  $k = 0, \dots, K-1$  and  $K$  odd. As can be seen, the goal now is to estimate the sequence  $f_n[k]$  obtained by sampling the pdf,  $f_n(\eta)$ . In terms of CFs, the goal is to estimate the CF, or equivalently, the *discrete Fourier transform* (DFT) of  $f_n[\cdot]$ , namely

$$F_n[m] = \sum_{k=-(K-1)/2}^{(K-1)/2} f_n[k] e^{-2\pi m k / K}, \quad (3.42)$$

for  $m = -(K-1)/2, \dots, (K-1)/2$ . However, the preamble method as developed in Section 3.3 only provides an estimate of the CF of  $f_n(\cdot)$ , i.e.,

$$\Phi_n(\omega) = \int_{-\infty}^{\infty} f_n(\eta) e^{-j\omega\eta} d\eta. \quad (3.43)$$

Thus, additional development of the preamble technique is required to show how an estimate of  $\Phi_n(\omega)$  can be used to construct an estimate of  $F_n[m]$ .

To begin, consider the FT of the sequence  $\tilde{f}_n[k] = f_n(k\Delta)$  for  $k$  from  $-\infty$  to  $\infty$ . The FT of this sequence is written as

$$\tilde{F}_n(e^{j\omega}) = \sum_{k=-\infty}^{\infty} \tilde{f}_n[k] e^{-j\omega k}. \quad (3.44)$$

Using the properties of the sampling theorem, it can be shown that [18]

$$\tilde{F}_n(e^{j\omega}) = \frac{1}{\Delta} \sum_{l=-\infty}^{\infty} \Phi_n \left( -\frac{\omega}{\Delta} + \frac{2\pi l}{\Delta} \right), \quad (3.45)$$

which is the infinite sum of shifted values of  $\Phi_n(\cdot)$ . Next, the desired sequence,  $f_n[k]$ , can be obtained from  $\tilde{f}_n[k]$  as

$$f_n[k] = \tilde{f}_n[k] \cdot h[k], \quad (3.46)$$

where  $h[k]$  is a window function given by

$$h[k] = \begin{cases} 1, & \text{for } k = -(K-1)/2, \dots, (K-1)/2 \\ 0, & \text{elsewhere.} \end{cases} \quad (3.47)$$

Using the Fourier transform properties,  $F_n(e^{j\omega})$ , the FT of  $f_n[k]$ , can be written as

$$F_n(e^{j\omega}) = \tilde{F}_n(e^{j\omega}) * H(e^{j\omega}), \quad (3.48)$$

where

$$H(e^{j\omega}) = \frac{\sin(\omega K/2)}{\sin(\omega/2)}, \quad (3.49)$$

and  $*$  denotes convolution. Combining Eq. (3.45) with Eq. (3.48),  $F_n(e^{j\omega})$  is given by

$$F_n(e^{j\omega}) = \frac{\sin(\omega K/2)}{\Delta \sin(\omega/2)} * \sum_{l=-\infty}^{\infty} \Phi_n \left( -\frac{\omega}{\Delta} + \frac{2\pi l}{\Delta} \right). \quad (3.50)$$

Finally,  $F_n(m)$ , the DFT of  $f_n[k]$ , can be obtained from  $F_n(e^{j\omega})$ , the FT of  $f_n[k]$ , using the relationship [18]

$$F_n[m] = F_n(e^{j\omega}) \big|_{\omega=2\pi m/K}, \quad (3.51)$$

yielding the result,

$$F_n[m] = \frac{1}{2\pi\Delta} \sum_{l=-\infty}^{\infty} \int_{-\pi}^{\pi} \frac{\sin(\lambda K/2)}{\sin(\lambda/2)} \Phi_n \left( \frac{\lambda}{\Delta} - \frac{2\pi}{\Delta} \left( \frac{m}{K} - l \right) \right) d\lambda. \quad (3.52)$$

To make the relationship between  $F_n[\cdot]$  and  $\Phi_n(\cdot)$  given in Eq. (3.52) more tractable, two simplifying approximations can be used. First, for the case when  $K$  is sufficiently large, the windowing effect of  $h[\cdot]$  will become negligible, and

$$\frac{1}{2\pi} \int_{-\pi}^{\pi} \frac{\sin(\lambda K/2)}{\sin(\lambda/2)} \Phi_n \left( \frac{\lambda}{\Delta} - \frac{2\pi}{\Delta} \left( \frac{m}{K} - l \right) \right) d\lambda \rightarrow \Phi_n \left( -\frac{2\pi}{\Delta} \left( \frac{m}{K} - l \right) \right). \quad (3.53)$$

Second, for most CFs of interest that decay to zero as  $\omega$  increases, the infinite summation in Eq. (3.52) can be approximated by a finite summation. Given these two approximations, Eq. (3.52) becomes

$$F_n[m] \approx \frac{1}{\Delta} \sum_{l=-M}^M \Phi_n \left( -\frac{2\pi}{T} (m - lK) \right), \quad (3.54)$$

for  $m = -(K-1)/2, \dots, (K-1)/2$  and  $K$  odd, where  $T = K\Delta$  is the support width of the histogram, and  $M$  is called the “aliasing factor.”

Recall that the preamble method was derived using the simplifying assumption that  $f_n(\eta)$  is an even symmetric pdf, causing  $f_n[k]$  to be even symmetric as well. In this case, it is readily observed that

$$\Phi_n(\omega) = \Phi_n(-\omega), \quad (3.55)$$

and

$$F_n[m] = F_n[-m]. \quad (3.56)$$

As a result, for the case of even symmetric pdfs it is sufficient to estimate  $F_n[m]$  for  $m = 0, \dots, (K-1)/2$ .

In conclusion, given the assumptions and approximations specified in this section and Section 3.3, the preamble method for enhancing the histogram LO detector can be summarized as follows:

1. Determine values for the parameters  $K$  (number of histogram bins),  $T$  (the support width of the histogram), and  $M$  (the aliasing factor).
2. Compute  $\hat{\Phi}_n(\omega_0(m - lK))$  using Eq. (3.34) for  $m = 0, \dots, (K-1)/2$  and  $l = -M, \dots, M$ , where  $\omega_0 = 2\pi/T$ .

3. Estimate  $F_n[m]$  as

$$\hat{F}_n[m] = \frac{1}{\Delta} \sum_{l=-M}^M \hat{\Phi}_n(\omega_0(m - lK)), \quad (3.57)$$

for  $m = 0, \dots, (K - 1)/2$ .

4. Determine the histogram levels,  $l_k = \hat{f}_n[k - (K - 1)/2]$ , by computing the inverse DFT of the sequence

$$\{\hat{F}_n[(K - 1)/2], \dots, \hat{F}_n[1], \hat{F}_n[0], \hat{F}_n[1], \dots, \hat{F}_n[(K - 1)/2]\}.$$

5. Form the histogram LO nonlinearity using the histogram found in Step 4 and the method discussed in Section 2.1.

Figure 3.20 to Fig. 3.26 depict various stages of the histogram LO detector algorithm for the case of Laplace noise and system parameters  $K = 15$ ,  $T = 30$ ,  $M = 1$ ,  $Q = 20,000$ , and  $E_c/\sigma = 0$  dB. Laplace noise, rather than Cauchy noise, was chosen so as to illustrate the “robustness” of the robust LO detector. A typical histogram estimate of the received signal pdf for this scenario is provided in Fig. 3.20. Two histogram estimates of the noise pdf, one formed using uncorrupted noise samples, and the other constructed using the preamble technique, are given in Fig. 3.21 and Fig. 3.22, respectively. The desired histogram LO nonlinearity, implemented using uncorrupted noise samples, is shown in Fig. 3.23, and the corresponding histogram LO nonlinearity estimated using the received signal samples is provided in Fig. 3.24. As can be seen from this figure, the nonlinearity estimated using the received signal samples possesses an undesired inflection in the region centered about the origin. The histogram LO nonlinearity estimated using the preamble technique, however, does not have this inflection, as illustrated in Fig. 3.25. Furthermore, this nonlinearity estimate is a close approximation of the desired nonlinearity in Fig. 3.23. Finally, Fig. 3.26 shows the preamble estimated DFT of the noise histogram that was used to construct the LO nonlinearity of Fig. 3.25. As can be seen, the estimate closely approximates the theoretical DFT obtained given knowledge of the mathematical expression for the noise pdf. For further analysis of the preamble technique for histogram LO detection, see Chapter 4 of this report.

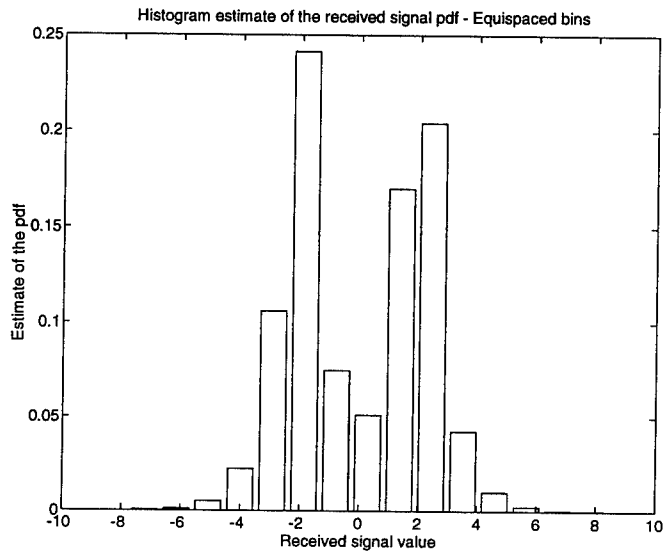


Figure 3.20: Histogram estimate of the received signal pdf,  $K = 15$ ,  $T = 30$ ,  $Q = 20,000$ ,  $E_c/\sigma = 0 \text{ dB}$ .

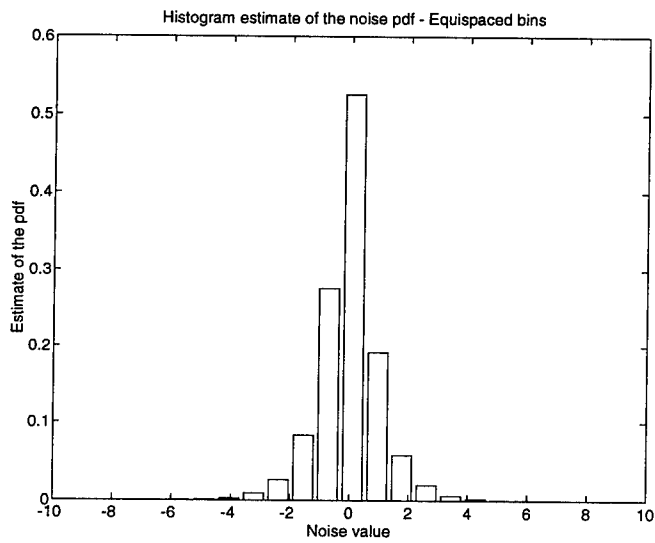


Figure 3.21: Histogram estimate of the noise pdf,  $K = 15$ ,  $T = 30$ ,  $Q = 20,000$ ,  $E_c/\sigma = 0 \text{ dB}$ .



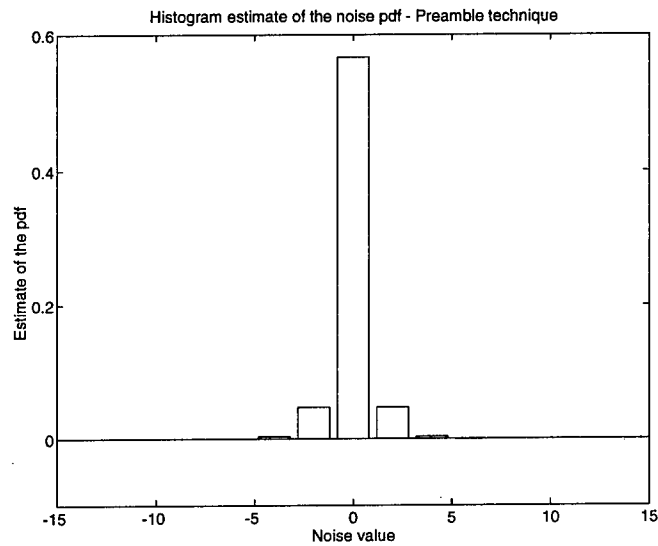


Figure 3.22: Preamble enhanced histogram estimate of the noise pdf,  $K = 15$ ,  $T = 30$ ,  $M = 1$ ,  $Q = 20,000$ ,  $E_c/\sigma = 0 \text{ dB}$ .

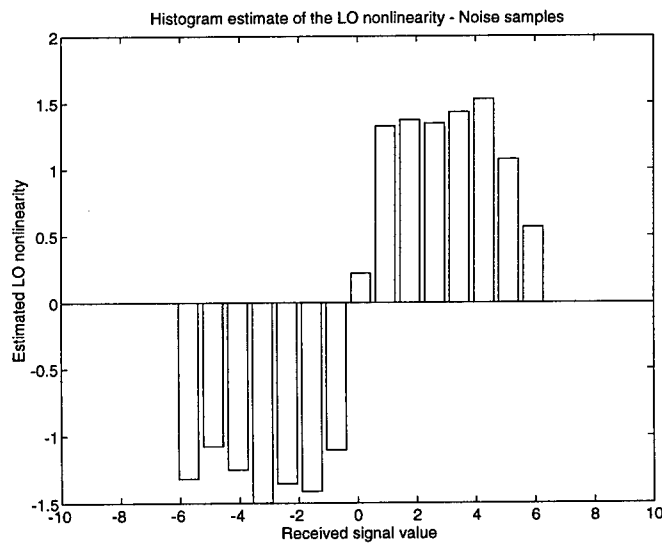


Figure 3.23: Histogram estimate of the LO nonlinearity using noise samples,  $K = 15$ ,  $T = 30$ ,  $Q = 20,000$ ,  $E_c/\sigma = 0 \text{ dB}$ .

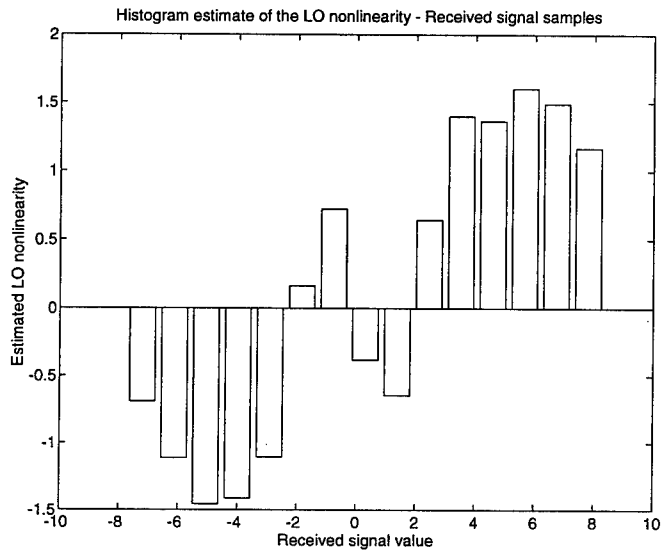


Figure 3.24: Histogram estimate of the LO nonlinearity using received signal samples,  $K = 15$ ,  $T = 30$ ,  $Q = 20,000$ ,  $E_c/\sigma = 0 \text{ dB}$ .

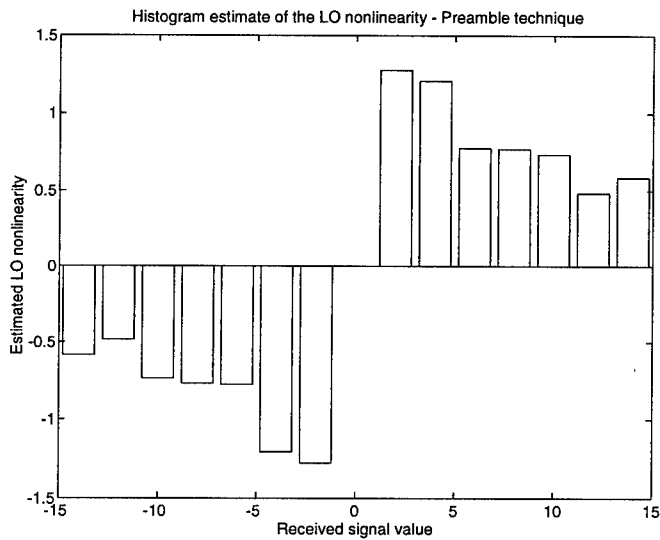


Figure 3.25: Preamble enhanced histogram estimate of the LO nonlinearity,  $K = 15$ ,  $T = 30$ ,  $M = 1$ ,  $Q = 20,000$ ,  $E_c/\sigma = 0 \text{ dB}$ .

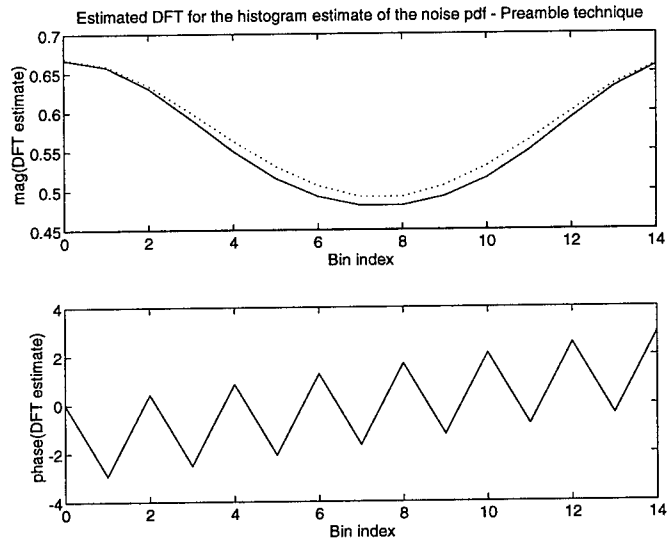


Figure 3.26: Estimate of the histogram DFT using the preamble technique,  $K = 15$ ,  $T = 30$ ,  $M = 1$ ,  $Q = 20,000$ ,  $E_c/\sigma = 0 \text{ dB}$ . Legend: — Preamble enhancement, .... Theoretical

### 3.3.3 The Variance of the Estimator $\hat{\Phi}_n(k\omega_0)$

Of critical importance in attaining a reliable estimate of  $\Phi_n(k\omega_0)$  is determining the number of observations,  $Q$ , used to compute the estimate

$$\hat{\Phi}_n(k\omega_0) = \frac{1}{Q} \sum_{j=1}^Q \cos(k\omega_0\eta_j). \quad (3.58)$$

One method is to choose  $Q$  such that the variance of  $\hat{\Phi}_n(k\omega_0)$  is less than some fraction,  $\alpha$ , of the quantity  $\Phi_n^2(k\omega_0)$ . Denoting the expected value and variance of an estimator as  $E\{\cdot\}$  and  $Var\{\cdot\}$ , respectively, it is well known that [16]

$$Var\{\hat{\Phi}_n(k\omega_0)\} = E\{\hat{\Phi}_n^2(k\omega_0)\} - [E\{\hat{\Phi}_n(k\omega_0)\}]^2. \quad (3.59)$$

The expected value of  $\hat{\Phi}_n(k\omega_0)$  is

$$E\{\hat{\Phi}_n(k\omega_0)\} = \frac{1}{Q} \sum_{j=1}^Q E\{\cos(k\omega_0\eta_j)\} = E\{\cos(k\omega_0\eta_j)\} = \Phi_n(k\omega_0), \quad (3.60)$$

for  $\{\eta_j\}$  iid. Next,  $E\{\hat{\Phi}_n^2(k\omega_0)\}$  is given by

$$E\{\hat{\Phi}_n^2(k\omega_0)\} = \frac{1}{Q^2} \sum_{i=1}^Q \sum_{j=1}^Q E\{\cos(k\omega_0\eta_i) \cos(k\omega_0\eta_j)\}. \quad (3.61)$$

For the case when  $i \neq j$ , with  $\{\eta_j\}$  iid,

$$\begin{aligned} E\{\cos(k\omega_0\eta_i) \cos(k\omega_0\eta_j)\} &= E\{\cos(k\omega_0\eta_i)\} E\{\cos(k\omega_0\eta_j)\} \\ &= \Phi_n^2(k\omega_0). \end{aligned} \quad (3.62)$$

When  $i = j$ , the expression in Eq. (3.62) becomes

$$\begin{aligned} E\{\cos(k\omega_0\eta_i) \cos(k\omega_0\eta_j)\} &= E\{\cos^2(k\omega_0\eta_j)\} = \frac{1}{2} E\{1 + \cos(2k\omega_0\eta_j)\} \\ &= \frac{1}{2} + \frac{1}{2} \Phi_n(2k\omega_0). \end{aligned} \quad (3.63)$$

Substituting Eq. (3.62) and Eq. (3.63) into Eq. (3.61),  $E\{\hat{\Phi}_n^2(k\omega_0)\}$  becomes

$$\begin{aligned} E\{\hat{\Phi}_n^2(k\omega_0)\} &= \frac{1}{Q^2}Q \left[ \frac{1}{2} + \frac{1}{2}\Phi_n(2k\omega_0) \right] + \frac{1}{Q^2}(Q^2 - Q)\Phi_n^2(k\omega_0) \\ &= \frac{1}{2Q}[1 + \Phi_n(2k\omega_0)] + \left(1 - \frac{1}{Q}\right)\Phi_n^2(k\omega_0). \end{aligned} \quad (3.64)$$

Finally, substituting Eq. (3.60) and Eq. (3.64) in Eq. (3.59), it can be shown that

$$\text{Var}\{\hat{\Phi}_n(k\omega_0)\} = \frac{1}{2Q}[1 + \Phi_n(2k\omega_0) - 2\Phi_n^2(k\omega_0)]. \quad (3.65)$$

As examples, consider the cases of LO detection in three different noise environments: Cauchy noise, Gaussian noise, and Laplace noise. For the case of Cauchy noise,

$$f_n(\eta) = \frac{\sigma}{\pi} \frac{1}{\sigma^2 + \eta^2}, \quad \sigma > 0, \quad (3.66)$$

and

$$\Phi_n(k\omega_0) = e^{-\sigma\omega_0|k|}, \quad \omega_0 > 0. \quad (3.67)$$

Substituting Eq. (3.67) in Eq. (3.65), it can be shown that, for Cauchy noise,

$$\text{Var}\{\hat{\Phi}_n(k\omega_0)\} = \frac{1}{2Q} [1 - e^{-2\sigma\omega_0|k|}], \quad (3.68)$$

which is monotonically increasing for  $k > 0$ , with

$$\text{Var}\{\hat{\Phi}_n(0)\} = 0 \quad (3.69)$$

$$\lim_{k \rightarrow \infty} \text{Var}\{\hat{\Phi}_n(k\omega_0)\} = \frac{1}{2Q}. \quad (3.70)$$

In the case of Gaussian noise,

$$f_n(\eta) = \frac{1}{\sqrt{2\pi}\sigma^2} e^{-\eta^2/(2\sigma^2)}, \quad \sigma > 0, \quad (3.71)$$

and

$$\Phi_n(k\omega_0) = e^{-\frac{1}{2}k^2\omega_0^2\sigma^2}, \quad \omega_0 > 0. \quad (3.72)$$

Substituting Eq. (3.72) in Eq. (3.65), it can be shown that, for Gaussian noise,

$$\text{Var}\{\hat{\Phi}_n(k\omega_0)\} = \frac{1}{2Q} [1 - e^{-k^2\omega_0^2\sigma^2}]^2, \quad (3.73)$$

which is monotonically increasing for  $k > 0$ , with

$$\text{Var}\{\hat{\Phi}_n(0)\} = 0 \quad (3.74)$$

$$\lim_{k \rightarrow \infty} \text{Var}\{\hat{\Phi}_n(k\omega_0)\} = \frac{1}{2Q}. \quad (3.75)$$

Finally, for the case of Laplace noise,

$$f_n(\eta) = \frac{1}{\sqrt{2}\sigma^2} e^{-\sqrt{\frac{2}{\sigma^2}}|\eta|}, \quad \sigma > 0, \quad (3.76)$$

and

$$\Phi_n(k\omega_0) = \frac{2}{2 + (\sigma\omega_0 k)^2}, \quad \omega_0 > 0. \quad (3.77)$$

Again, substituting Eq. (3.77) in Eq. (3.65), it can be shown that, for Laplace noise,

$$\text{Var}\{\hat{\Phi}_n(k\omega_0)\} = \frac{1}{2Q} \frac{2\sigma^4\omega_0^4 k^4 (\sigma^2\omega_0^2 k^2 + 5)}{(2\sigma^2\omega_0^2 k^2 + 1)(\sigma^4\omega_0^4 k^4 + 4\sigma^2\omega_0^2 k^2 + 4)}. \quad (3.78)$$

As before, it is readily seen that

$$\text{Var}\{\hat{\Phi}_n(0)\} = 0 \quad (3.79)$$

$$\lim_{k \rightarrow \infty} \text{Var}\{\hat{\Phi}_n(k\omega_0)\} = \frac{1}{2Q}. \quad (3.80)$$

However, for the case of Laplace noise,  $\text{Var}\{\hat{\Phi}_n(k\omega_0)\}$  is not a monotonically increasing function for  $k > 0$ . Rather, using Mathcad<sup>TM</sup> by MathSoft, Inc., the expression in Eq. (3.78) can be shown to have a maximum value at  $k = \left(\sqrt{13 + 3\sqrt{21}}\right)/(\sigma\omega_0)$ . For  $k$  equal to this value,  $\text{Var}\{\hat{\Phi}_n(k\omega_0)\} \approx (1.008669985)/(2Q)$ , a number slightly larger than  $1/(2Q)$ .

To compare the number of samples required in the different noise environments, consider the criterion of choosing  $Q$  such that the variance of the CF estimator at  $k\omega_0$  is less than some fraction of the square of the actual CF at  $k\omega_0$ , i.e., choose  $Q$  such that

$$\text{Var}\{\hat{\Phi}_n(k\omega_0)\} < \alpha \Phi_n^2(k\omega_0). \quad (3.81)$$

Noting that for Cauchy, Gaussian, and Laplace noise,  $Var\{\hat{\Phi}_n(k\omega_0)\}$  approaches  $1/(2Q)$  as  $k$  approaches infinity, one can choose  $Q$  such that

$$Q > \frac{1}{2\alpha\Phi_n^2(k_{max}\omega_0)}, \quad (3.82)$$

where  $k_{max}$  is the largest  $k$  for which  $\hat{\Phi}_n(k\omega_0)$  is to be computed. Substituting the corresponding expressions for  $\Phi_n(\cdot)$  into Eq. (3.82), the respective requirements on  $Q$  for the different noise types become:

- For Cauchy noise:

$$Q > \frac{e^{2\sigma\omega_0|k_{max}|}}{2\alpha} \quad (3.83)$$

- For Gaussian noise:

$$Q > \frac{e^{k_{max}^2\omega_0^2\sigma^2}}{2\alpha} \quad (3.84)$$

- For Laplace noise:

$$Q > \frac{[2 + (k_{max}\omega_0\sigma)^2]^2}{8\alpha}. \quad (3.85)$$

As a specific example, consider the implementation of the FSA LO detector having order  $p$  and support  $T = 50$ . Thus,  $k_{max} = 2p$  and  $\omega_0 = (2\pi)/T = \pi/25$ . For the case when the noise parameters are all  $\sigma = 1$  and  $\alpha = 1/8$ , Eq. (3.83) through Eq. (3.85) become

- For Cauchy noise:

$$Q > 4e^{\frac{4\pi}{25}p} \quad (3.86)$$

- For Gaussian noise:

$$Q > 4e^{\left(\frac{2\pi}{25}\right)^2 p^2} \quad (3.87)$$

- For Laplace noise:

$$Q > \left[2 + \left(\frac{2\pi}{25}\right)^2 p^2\right]^2, \quad (3.88)$$

Plots of  $Q_{min}$  relative to  $p$  are provided in Fig. 3.27 that indicate how the type of noise directly influences the number of samples required to provide a reliable estimate of the corresponding LO nonlinearity. Furthermore, this example, in conjunction with the material presented in this section, clearly illustrates how the variance of the estimator  $\hat{\Phi}_n(k\omega_0)$  can be used to gauge the accuracy of a preamble enhanced robust LO nonlinearity in terms of the number of samples utilized in the estimation process.

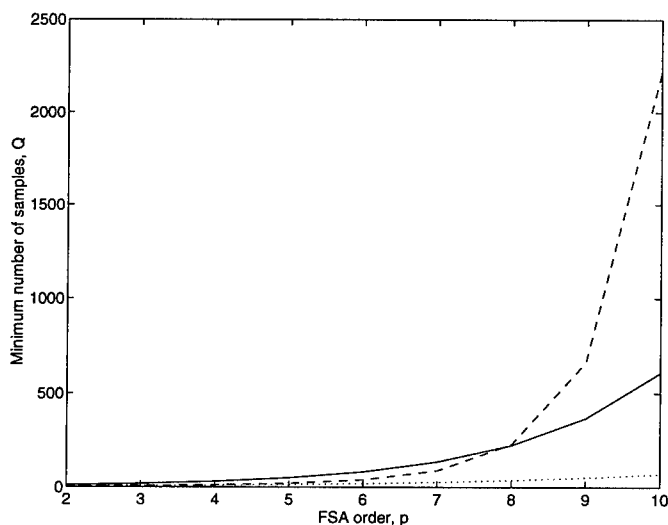


Figure 3.27: Number of samples,  $Q$ , required relative to the FSA order,  $p$ , indicated by the preamble technique variance criterion. Legend: — Cauchy noise, - - Gaussian noise, .... Laplace noise



## Chapter 4

# Performance Analysis

One method that has proven useful in quantifying the performance of robust LO detectors is Monte Carlo simulation analysis. In this study, two Matlab<sup>TM</sup> computer simulations were implemented for examining the characteristics of the various enhancement algorithms presented in Chapter 3. One program simulates the histogram robust LO detector in a *direct sequence* (DS) *spread spectrum* (SS) BPSK system, while the other simulates a BPSK DSSS system employing an FSA robust LO detector. In both simulations, the system can be subjected to one of three types of channel interference: iid Cauchy noise, iid Laplace noise, or iid Gaussian noise. Furthermore, each simulation compares the enhanced robust LO detector in question to:

- the theoretical LO detector (known pdf case)
- the robust LO detector using noise samples for estimation (ideal case)
- the robust LO detector using received signal samples for estimation (large  $J/S$  implementation)
- the linear detector.

Thus, the remainder of this chapter examines the *probability of bit error* ( $P_b$ ) for the different detector/enhancement combinations, facilitating the comparison of detector effectiveness for different interference and enhancement scenarios.

## 4.1 Results for the Histogram Robust LO Detector

This section presents the simulation results for the histogram robust LO detector in conjunction with the following enhancement methods:

- the LS enhancement technique
- the CF enhancement technique
- the preamble enhancement technique.

As will be seen, both the LS and CF enhanced detectors, while typically providing a lower  $P_b$  than the standard large  $J/S$  implementation of the LO detector, exhibit performance degradation caused by the “binning” (or quantization) of the information signal’s amplitude. The preamble enhanced LO detector, on the other hand, does not exhibit this degradation in performance, and usually achieves a significantly lower  $P_b$  than does the large  $J/S$  implementation. However, as in all the enhancement algorithms, care must be taken in choosing appropriate values for the various system parameters.

### 4.1.1 The LS Enhancement Technique

To investigate the performance characteristics of the LS enhanced histogram LO detector,  $P_b$  curves for this detector in Cauchy noise are shown in Fig. 4.1 to Fig. 4.5, with a legend provided in Fig. 4.6. After an examination of the figures, a number of observations can be made concerning the detector performance. First, the LS enhanced LO detector performs better, in general, than the robust LO detector using the received signal samples.<sup>1</sup> Second, the performance of the LS enhanced detector for large  $E_c/\sigma$  improves as the histogram width,  $T$ , increases. However, increasing  $T$  decreases performance for low  $E_c/\sigma$  regions, illustrating an important performance trade-off. Finally, the  $P_b$  curves for the LS enhanced detector are not “smooth” functions of  $E_c/\sigma$ , and in fact, exhibit severe performance fluctuations.

---

<sup>1</sup>For these and subsequent curves,  $P_b$  is calculated by dividing the number of observed errors by the total number of bits transmitted. Thus, values of zero often are computed for an actual  $P_b$  that is less than or approximately equal to the number of transmitted bits. Since  $P_b$  is plotted on a logarithmic scale in the figures, values of zero are indicated by a break in the appropriate curve.

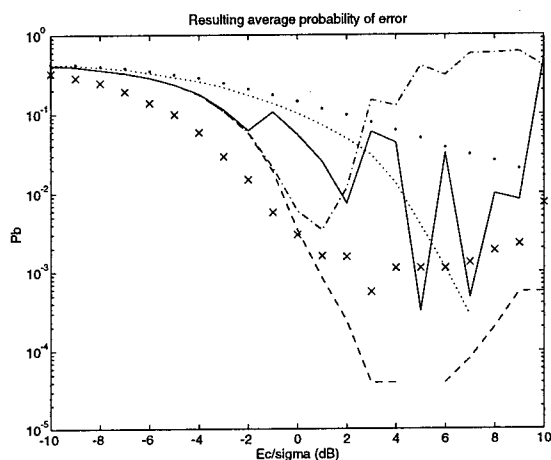


Figure 4.1:  $P_b$  curves for the LS enhanced histogram LO detector with  $N = 10$  samples per bit,  $K = 33$  histogram bins, filter length  $2L - 1 = 99$ , truncation width of  $T = 100$ , and  $Q = 50,000$  samples per pdf approximation.

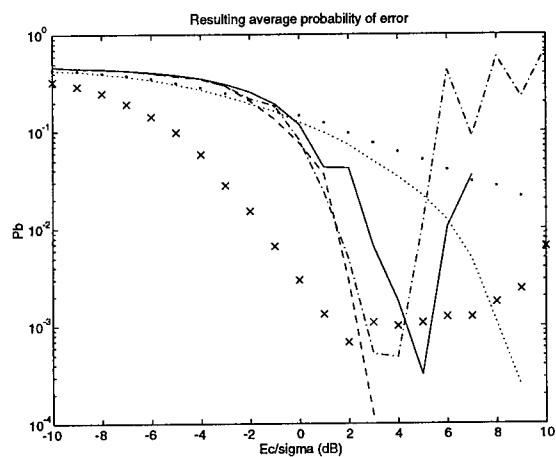


Figure 4.2:  $P_b$  curves for the LS enhanced histogram LO detector with  $N = 10$  samples per bit,  $K = 33$  histogram bins, filter length  $2L - 1 = 99$ , truncation width of  $T = 200$ , and  $Q = 50,000$  samples per pdf approximation.

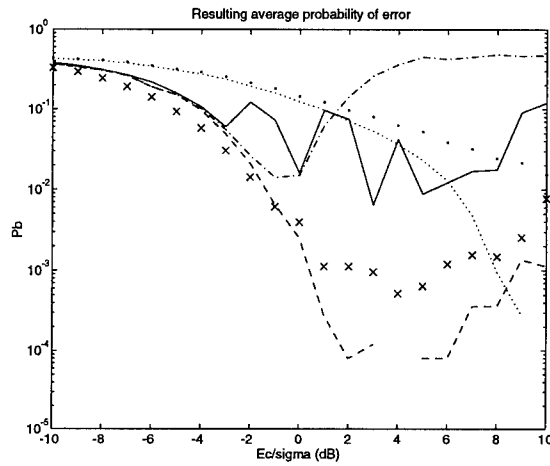


Figure 4.3:  $P_b$  curves for the LS enhanced histogram LO detector with  $N = 10$  samples per bit,  $K = 99$  histogram bins, filter length  $2L - 1 = 199$ , truncation width of  $T = 200$ , and  $Q = 50,000$  samples per pdf approximation.

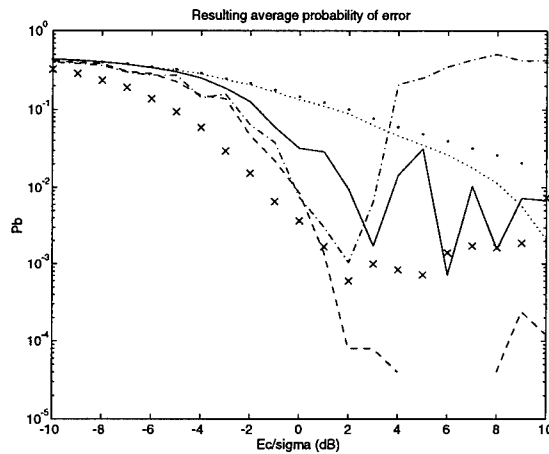


Figure 4.4:  $P_b$  curves for the LS enhanced histogram LO detector with  $N = 10$  samples per bit,  $K = 99$  histogram bins, filter length  $2L - 1 = 199$ , truncation width of  $T = 400$ , and  $Q = 50,000$  samples per pdf approximation.

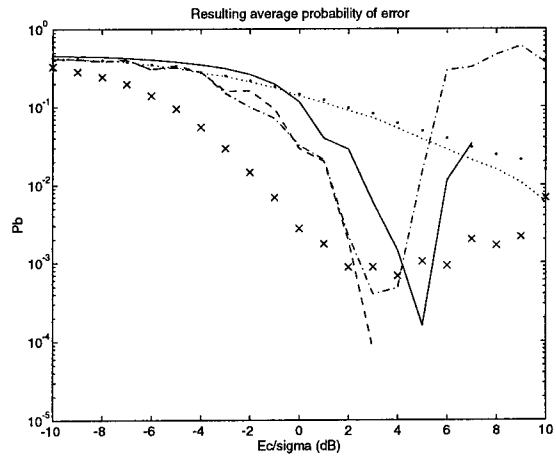


Figure 4.5:  $P_b$  curves for the LS enhanced histogram LO detector with  $N = 10$  samples per bit,  $K = 99$  histogram bins, filter length  $2L - 1 = 199$ , truncation width of  $T = 600$ , and  $Q = 50,000$  samples per pdf approximation.

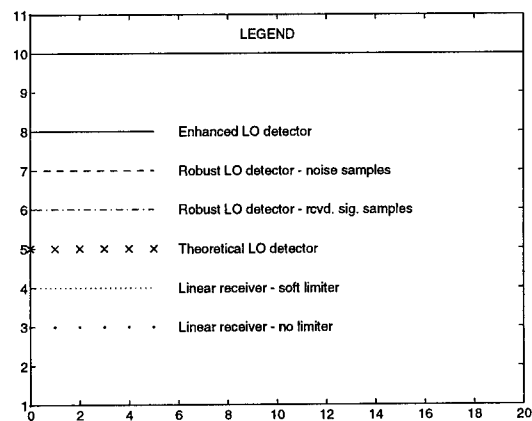


Figure 4.6: Legend for the probability of bit error figures.

Further analysis of the results for the LS enhanced detector revealed the cause of the performance fluctuations. Figure 4.7 shows a typical plot of  $P_b$  relative to the information signal amplitude,  $a$ . In addition, the bin endpoints for the received signal histogram are indicated by the "X" marks. As can be seen, local  $P_b$  minima occur when  $a$  lies in the center of a bin, and  $P_b$  increases for values of  $a$  close to the bin endpoints. The location of  $a$  in a histogram bin is critical for the following reasons. When  $a$  is located near the center of a bin, the bin index  $k_a$  accurately represents  $a$  and the resulting deconvolution filter,  $h$ , is closely related to the true information signal pdf. However, when  $a$  lies near a bin endpoint,  $k_a$  no longer accurately represents  $a$ , and the resulting deconvolution filter no longer corresponds to the true information signal pdf. Thus, an increase in pdf estimation error occurs when  $k_a$  does not accurately represent  $a$ , and is an inherent limitation possessed by the LS enhancement technique.

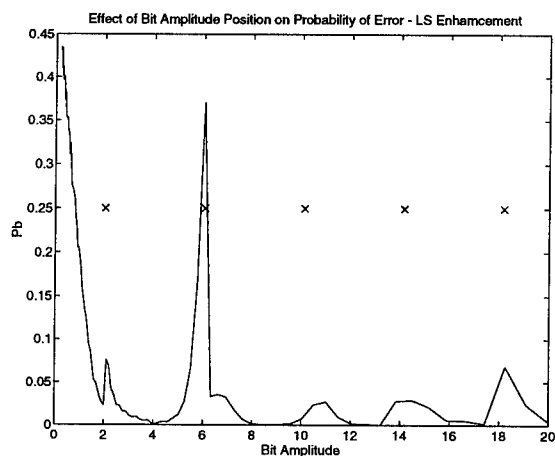


Figure 4.7: Effect of bit amplitude position on  $P_b$  for the LS enhanced robust LO detector.

#### 4.1.2 The CF Enhancement Technique

Representative  $P_b$  curves for the CF enhanced histogram LO detector subjected to iid Cauchy noise are provided in Fig. 4.8 and Fig. 4.9 (see Fig. 4.6

for a legend). Of particular interest is the fluctuations observed in the performance curves for the CF enhanced detector. As in the case of the LS enhanced LO detector, these fluctuations are directly related to the location of the BPSK signal amplitude,  $a$ , in a given histogram bin, indexed by  $k_a$ . This phenomenon can be readily observed in Fig. 4.10, a typical plot of  $P_b$  relative to  $a$ , and is a function of the relationship given in Eq. (3.20).

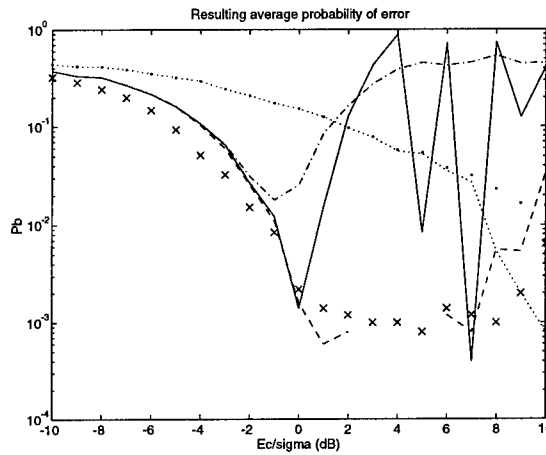


Figure 4.8:  $P_b$  curves for the CF enhanced histogram LO detector with  $N = 10$  samples per bit,  $K = 99$  histogram bins, truncation width of  $T = 200$ , and  $Q = 50,000$  samples per pdf approximation.

To understand the cause of the performance fluctuations, consider the following. Recall that the FT of the received signal pdf for a BPSK system is given by

$$F_r(e^{j\omega}) = F_n(e^{j\omega}) \cos(\omega a). \quad (4.1)$$

Assume that  $F_r(e^{j\omega})$  is known exactly, i.e., ignore the effects of histogram estimation error. Then, if the BPSK signal amplitude is approximated at the detector by  $k_a \Delta$ , where  $\Delta$  is the histogram bin width, Eq. (3.20) gives the following estimate of  $F_n(e^{j\omega})$ :

$$\hat{F}_n(e^{j\omega}) = F_n(e^{j\omega}) \frac{\cos(\omega a)}{\cos(\omega k_a \Delta)}. \quad (4.2)$$

Equation (4.2) clearly indicates that if  $k_a \Delta$  is not approximately equal to  $a$ , then  $\cos(\omega a)$  does not cancel  $\cos(\omega k_a \Delta)$ , which may lead to values of  $\omega$  for

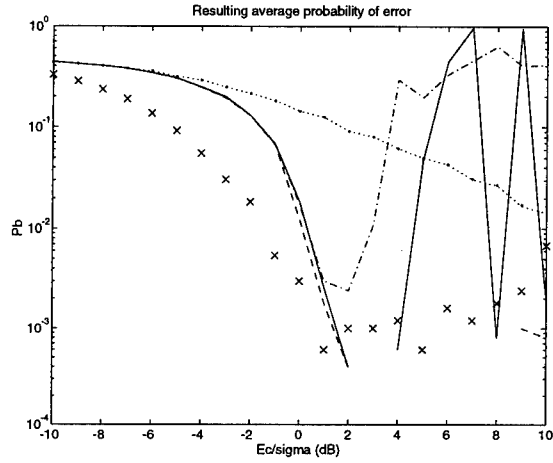


Figure 4.9:  $P_b$  curves for the CF enhanced histogram LO detector with  $N = 10$  samples per bit,  $K = 99$  histogram bins, truncation width of  $T = 400$ , and  $Q = 50,000$  samples per pdf approximation.

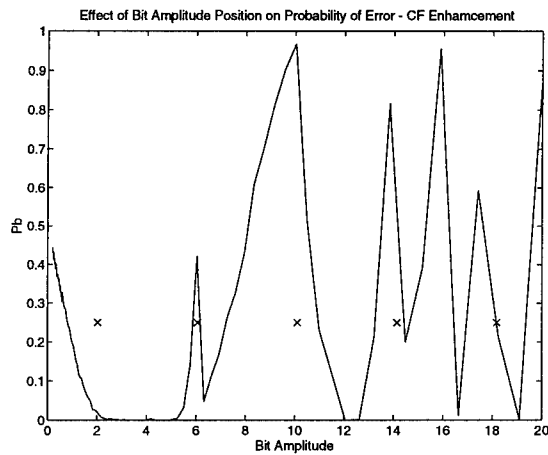


Figure 4.10: Effect of bit amplitude position on  $P_b$  for the CF enhanced robust LO detector.



which  $|\hat{F}_n(e^{j\omega})| \rightarrow \infty$  (or a very large number in computer simulations and applications). Thus, the performance of the CF enhancement technique is strongly dependent on the estimate of the information signal's amplitude at the detector.

### 4.1.3 The Preamble Enhancement Technique

To compare the performance of the preamble enhanced histogram LO detector to the LS and CF enhanced detectors, first consider the results provided in Fig. 4.11 for the case of Cauchy noise (see Fig. 4.6 for a legend). Two observations are immediately apparent after examining this figure and the figures in Section 4.1.1 and Section 4.1.2. First, the preamble enhanced LO detector provides a lower  $P_b$  than the corresponding large  $J/S$  implementation. Second, the preamble enhanced detector does not exhibit the performance fluctuations that are inherent to the LS and CF enhanced detectors. Thus, the *consistency* in performance of the preamble technique is a useful attribute for predicting detector effectiveness in a given interference environment.

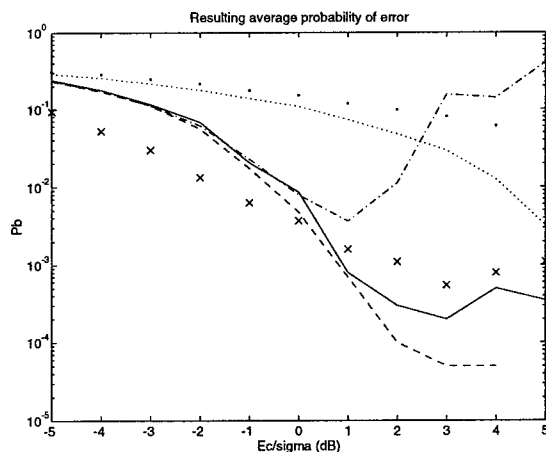


Figure 4.11:  $P_b$  curves for the preamble enhanced histogram LO detector in Cauchy noise with  $N = 10$  samples per bit,  $K = 33$  histogram bins, truncation width of  $T = 100$ , aliasing factor  $M = 1$ , and  $Q = 50,000$  samples per pdf approximation.

Given the promising results indicated in Fig. 4.11, an additional analy-

sis was performed to investigate further the preamble enhancement method. Figure 4.12 and Fig. 4.13 depict  $P_b$  curves for the preamble enhanced histogram LO detector subjected to Laplace noise, with aliasing factors  $M = 0$  and  $M = 1$ , respectively. For large values of  $E_c/\sigma$ , these figures illustrate the superior performance of the preamble enhanced detector as compared to the large  $J/S$  implementation. Conversely, for small values of  $E_c/\sigma$ , the preamble technique exhibits approximately a 1 dB degradation relative to the large  $J/S$  method. In many cases, however, this minor performance decrease may be a small price to pay given the increased range of reliable detection afforded by the preamble technique.

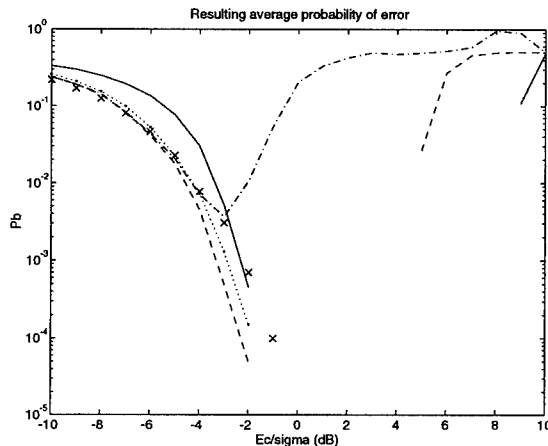


Figure 4.12:  $P_b$  curves for the preamble enhanced histogram LO detector in Laplace noise with  $N = 10$  samples per bit,  $K = 15$  histogram bins, truncation width of  $T = 30$ , aliasing factor  $M = 0$ , and  $Q = 20,000$  samples per pdf approximation.

## 4.2 Results for the FSA Robust LO Detector

This section presents the simulation results for the FSA robust LO detector in conjunction with the following enhancement methods:

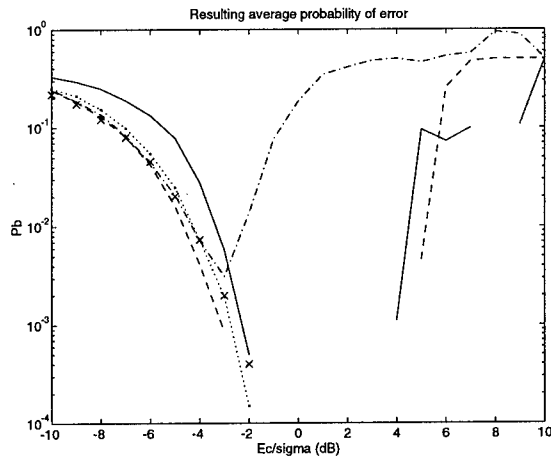


Figure 4.13:  $P_b$  curves for the preamble enhanced histogram LO detector in Laplace noise with  $N = 10$  samples per bit,  $K = 15$  histogram bins, truncation width of  $T = 30$ , aliasing factor  $M = 1$ , and  $Q = 20,000$  samples per pdf approximation.

- the CF enhancement technique
- the preamble enhancement technique.

Similar to the case of histogram LO detection, it will be seen that the preamble enhanced FSA LO detector typically exhibits better performance than the CF enhanced detector for a given interference scenario. However, one must keep in mind that this performance improvement is achieved at the expense of an increase in bandwidth overhead, which may or may not be an issue in a specific system implementation.

#### 4.2.1 The CF Enhancement Technique

Typical  $P_b$  curves for a CF enhanced FSA LO detector are given in Fig. 4.14 to Fig. 4.16 for the case of Cauchy interference. As in the case of histogram detection, the CF enhanced FSA detector also exhibits performance fluctuations as  $E_c/\sigma$  varies. This characteristic of the CF technique is directly related to the defining expression of Eq. (3.20), as was seen in the case of histogram detection discussed in Section 4.1.2.

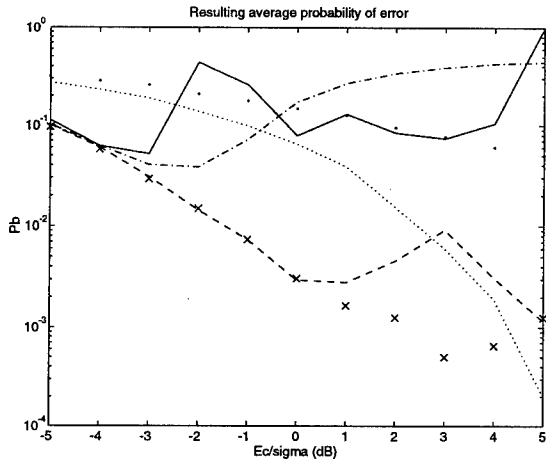


Figure 4.14:  $P_b$  curves for the CF enhanced FSA LO detector in Cauchy noise with  $N = 10$  samples per bit, FSA order of  $p = 10$ , truncation width of  $T = 50$  and  $Q = 20,000$  samples per nonlinearity approximation.

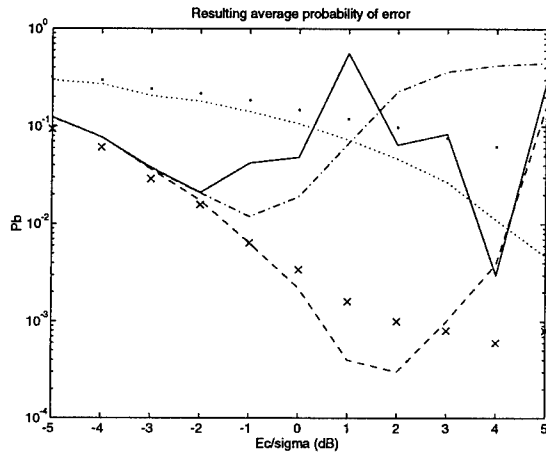


Figure 4.15:  $P_b$  curves for the CF enhanced FSA LO detector in Cauchy noise with  $N = 10$  samples per bit, FSA order of  $p = 10$ , truncation width of  $T = 100$  and  $Q = 20,000$  samples per nonlinearity approximation.

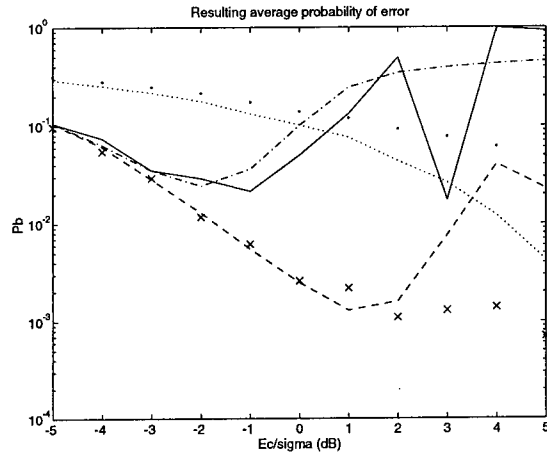


Figure 4.16:  $P_b$  curves for the CF enhanced FSA LO detector in Cauchy noise with  $N = 10$  samples per bit, FSA order of  $p = 15$ , truncation width of  $T = 100$  and  $Q = 20,000$  samples per nonlinearity approximation.

To determine the cause of these fluctuations in  $P_b$ , recall that the FSA LO nonlinearity is implemented using  $\hat{\Phi}_n(k\omega_0)$ , an estimate of the noise CF at multiples of  $\omega_0$ . If uncorrupted noise samples are available at the detector,  $\Phi_n(k\omega_0)$  can be estimated using the expression in Eq. (2.17), i.e.,

$$\hat{\Phi}_n(k\omega_0) = \frac{1}{Q} \sum_{j=1}^Q \cos(k\omega_0\eta_j), \quad (4.3)$$

where  $\{\eta_j\}$  is the set of  $Q$  observations of the noise. In CF enhanced detection, however, uncorrupted noise samples are *not* available. Instead, Eq. (3.20) is used to estimate  $\Phi_n(k\omega_0)$ , yielding the expression,

$$\hat{\Phi}_n(k\omega_0) = \frac{1}{Q} \frac{\sum_{j=1}^Q \cos(k\omega_0\eta_j)}{\cos(k\omega_0 a)}. \quad (4.4)$$

The expression in the numerator of Eq. (4.4) is an approximation of the received signal CF,  $\Phi_r(k\omega_0)$ , where

$$\Phi_r(k\omega_0) = \Phi_n(k\omega_0) \cos(k\omega_0 a), \quad (4.5)$$

and the term in the denominator of Eq. (4.4) attempts to cancel the  $\cos(k\omega_0 a)$  component of the expression in Eq. (4.5). However, since an approximation of  $\Phi_r(k\omega_0)$  is used, this cancellation is incomplete and manifests itself as an estimation error that is amplified for values of  $a$  such that  $\cos(k\omega_0 a)$  is small. This estimation error amplification produces a corresponding inaccuracy in the FSA nonlinearity, causing the performance fluctuations observed in Fig. 4.14 to Fig. 4.16.

## 4.2.2 The Preamble Enhancement Technique

This section presents the performance results for preamble enhanced FSA LO detection in Cauchy and Laplace noise environments. For the case of Cauchy noise, Fig. 4.17 to Fig. 4.20 provide  $P_b$  curves for the cases of  $Q = 30,000$  and  $Q = 60,000$  training samples, and different values for the FSA order,  $p$ , and approximation width,  $T$ . (See Fig. 4.6 for a legend.) These plots indicate that an increase in the number of training samples yields a decrease in  $P_b$ , as expected. However, it must be remembered that an increase in the number of training samples necessitates an increase in the overhead bandwidth of the system. Also, comparing Fig. 4.18 to Fig. 4.20 shows that increasing  $p$ , with an appropriate increase in  $T$ , improves performance provided that a sufficient number of observations are available for estimating the desired number of FSA coefficients.

Figure 4.21 shows example  $P_b$  curves for the case of FSA LO detection in Laplace noise (see Fig. 4.6 for a legend).<sup>2</sup> As in previous examples, the preamble enhanced detector provides a lower  $P_b$  than the corresponding large  $J/S$  implementation. Carrying the analysis further, an interesting comparison can be made between the FSA and histogram LO detectors. Comparing Fig. 4.21 with Fig. 4.12 and Fig. 4.13, it can be seen that the FSA detector provides better performance for low  $E_c/\sigma$ , whereas the histogram detector performs better in high  $E_c/\sigma$ . The reason for this trend is that the FSA algorithm produces a smooth, accurate estimate of the true LO nonlinearity for small values of the received signal, and thus the majority of received signal observations for low  $E_c/\sigma$ . On the other hand, for large values of the received signal, and thus the majority of received signal observations for high  $E_c/\sigma$ ,

<sup>2</sup>Note that the fluctuations in the performance curve for the preamble enhanced LO detector are caused by the relatively few samples used to compute  $P_b$ , and are *not* inherent to the preamble technique.

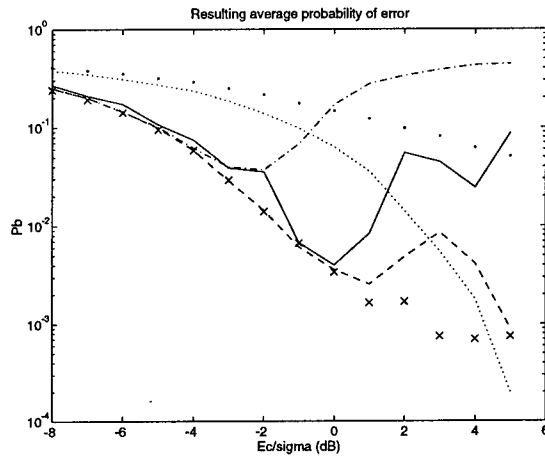


Figure 4.17:  $P_b$  curves for the preamble enhanced FSA LO detector in Cauchy noise with  $N = 10$  samples per bit, FSA order of  $p = 10$ , truncation width of  $T = 50$ , 20,000 samples per nonlinearity approx. (except preamble), and  $Q = 30,000$  training samples (corresponding to  $\alpha = 0.00254$ ).

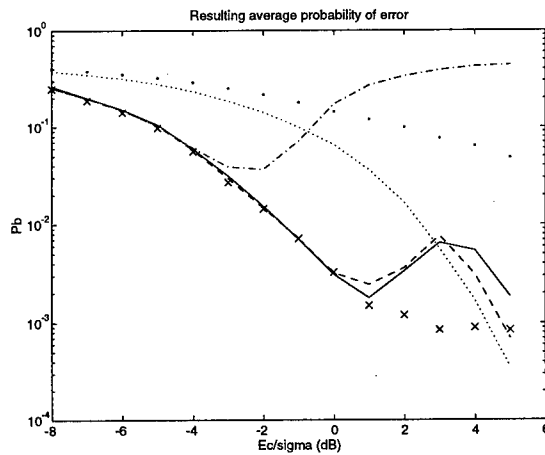


Figure 4.18:  $P_b$  curves for the preamble enhanced FSA LO detector in Cauchy noise with  $N = 10$  samples per bit, FSA order of  $p = 10$ , truncation width of  $T = 50$ , 20,000 samples per nonlinearity approx. (except preamble), and  $Q = 60,000$  training samples (corresponding to  $\alpha = 0.00127$ ).

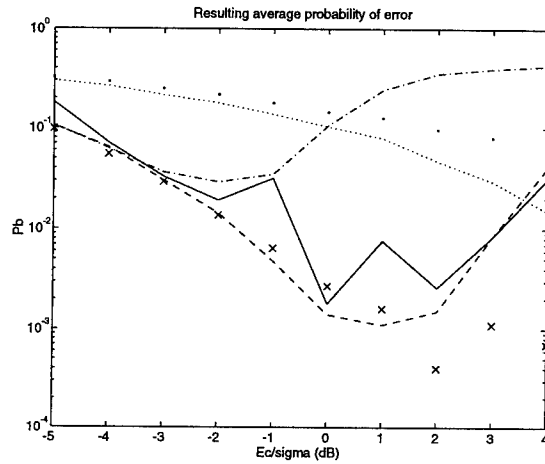


Figure 4.19:  $P_b$  curves for the preamble enhanced FSA LO detector in Cauchy noise with  $N = 10$  samples per bit, FSA order of  $p = 15$ , truncation width of  $T = 100, 20,000$  samples per nonlinearity approx. (except preamble), and  $Q = 30,000$  training samples (corresponding to  $\alpha = 0.000723$ ).

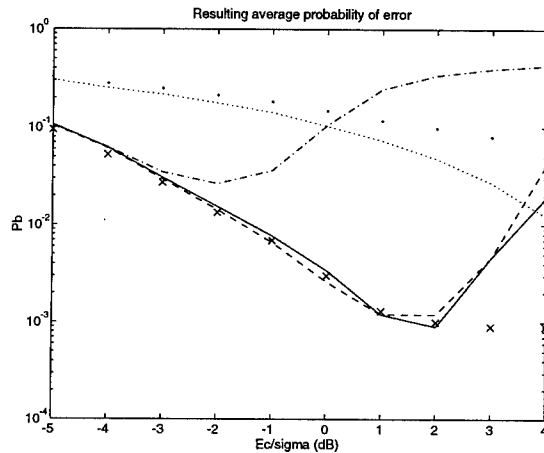


Figure 4.20:  $P_b$  curves for the preamble enhanced FSA LO detector in Cauchy noise with  $N = 10$  samples per bit, FSA order of  $p = 15$ , truncation width of  $T = 100, 20,000$  samples per nonlinearity approx. (except preamble), and  $Q = 60,000$  training samples (corresponding to  $\alpha = 0.000361$ ).



the estimated FSA LO nonlinearity exhibits the “ripples” inherent to the FSA algorithm, causing a decrease in nonlinearity approximation accuracy and a corresponding increase in  $P_b$ . With the addition of error correction coding, however, the difference in detector performance should become small. In this case, the choice of LO detector algorithm, e.g., histogram or FSA, will be determined by which is more amenable to a given system application.

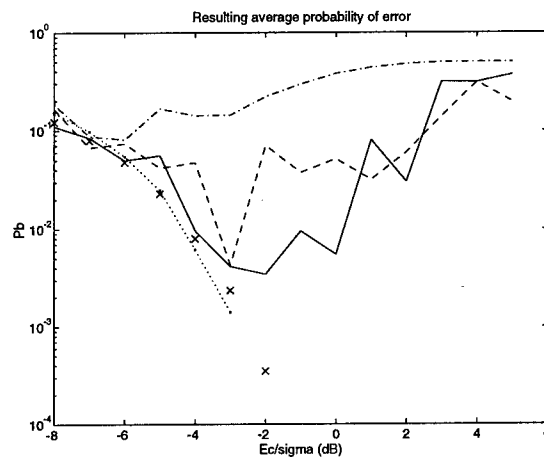


Figure 4.21:  $P_b$  curves for the preamble enhanced FSA LO detector in Laplace noise with  $N = 10$  samples per bit, FSA order of  $p = 10$ , truncation width of  $T = 30$ , 20,000 samples per nonlinearity approx. (except preamble), and  $Q = 60,000$  training samples (corresponding to  $\alpha = 7.96 \times 10^{-5}$ ).

# Chapter 5

## Summary and Future Research

The previous chapters identified and examined various enhancement techniques for use with indirect and direct robust LO detector algorithms. Moreover, simulation results indicate that with enhancement, the performance of the robust LO detector can approach that of the ideal case in which uncorrupted noise samples are used to estimate the LO nonlinearity. The methods developed herein, however, assume that the noise samples are *independent and identically distributed* (iid), which may not be indicative of the more correlated noise, e.g., narrowband interference, that is encountered in many applications. With this in mind, the remainder of the chapter summarizes the work presented in this report, and discusses the evolution of the research topic so as to address more complex noise environments.

### 5.1 Summary

This report represents the culmination of a study concerning enhancement methods for robust *locally optimum* (LO) signal detection. In Chapter 2, the LO detector for independent noise and the concept of *robust* LO detection were introduced. Also, two types of robust LO detectors, the histogram indirect implementation and the *Fourier series approximation* (FSA) direct implementation, were reviewed. With this framework in place, the focus of the research effort was discussed next in Chapter 3.

Chapter 3 presented the derivations of three robust LO detector enhancements: the *least squares* (LS), the *characteristic function* (CF), and the

preamble enhancement methods. In the LS method, a least squares deconvolution filter is used to obtain an estimate of the noise *probability density function* (pdf) from an estimate of the received signal pdf. The CF method utilizes the relationship between a pdf and its CF to obtain an estimate of the noise CF from an estimate of the received signal CF formed as a function of the received signal samples. One potential limitation that both the LS and CF enhancement techniques possess is that each requires an accurate estimate, at the *receiver*, of the transmitted information signal's amplitude. Since in many applications knowledge of this amplitude is unavailable at the receiver, another enhancement technique was developed, the preamble method. In the preamble method, training samples are used to compute an estimate of the noise CF (and the noise pdf, if necessary) from which an estimate of the LO nonlinearity is obtained.

Using the methods described in Chapter 3, Chapter 4 presents the performance results for several robust LO detector algorithm and enhancement technique combinations. It was observed that, in most cases, the enhanced LO detectors achieved lower probability of errors than the corresponding large *jammer-to-signal ratio* ( $J/S$ ) implementation of the LO detector.<sup>1</sup> Moreover, due to the limitations imposed by the transmitted signal amplitude estimation accuracy, the performance of the preamble enhanced LO detector was, in most cases, significantly better than corresponding LS or CF enhanced detector. However, it must be remembered that this performance improvement occurs at the expense of increasing the overhead bandwidth of the system, an important consideration in some applications. Table 5.1 summarizes some of the performance trade-offs for the various LO detector and enhancement technique combinations.

## 5.2 Future Research

With the insight gained from this report, the logical evolution of this research topic can be ascertained. Recall that the results presented herein were obtained under the assumption that the noise samples were *independent and identically distributed* (iid). However, in many scenarios of interest the in-

---

<sup>1</sup>In the large  $J/S$  LO detector implementation, the received signal samples are assumed to be approximately equal to the noise samples. Thus, the received signal samples are used to estimate the desired LO nonlinearity.

Enhanced Robust LO Detector Characteristics				
Enhanced LO detector type	Parameters to be determined	Increased overhead bandwidth	Signal amplitude required	Performance fluctuations observed
LS enhanced histogram LO detector	$K, T, Q, L$		X	X
CF enhanced histogram LO detector	$K, T, Q$		X	X
Preamble enhanced histogram LO detector	$K, T, Q$	X		
CF enhanced FSA LO detector	$p, T, Q$		X	X
Preamble enhanced FSA LO detector	$p, T, Q$	X		

Table 5.1: Performance characteristics and trade-offs for the various robust LO detector algorithm and enhancement technique combinations examined in this report. Parameters:  $K$  is the number of histogram bins,  $p$  is the FSA order,  $T$  is the LO nonlinearity approximation width (support),  $Q$  is the number of samples per nonlinearity approximation, and  $L$  is the length parameter for the LS method deconvolution filter. Note, an "X" indicates that the detector possesses the corresponding characteristic.

terference is not iid, and in fact, is highly correlated, e.g., as in the case of narrowband interference. Thus, means should be identified for applying the methods examined in this study to more general noise types.

One method that may achieve this goal is to model the noise as an *auto-regressive* (AR) process. For a first-order AR process, the noise samples,  $\{n_i\}$ , are modeled as

$$n_i = a n_{i-1} + w_i, \quad (5.1)$$

where  $\{w_i\}$  is an iid noise sequence, and  $a$  is a constant parameter related to the correlation of the noise. Given the expression in Eq. (5.1), it can be shown that the LO detector for first-order AR noise is [19]

$$l(\rho) = \sum_{i=1}^N (s_{1i} - s_{0i}) g_i(\rho) \begin{array}{l} \text{choose } H_1 \\ > \\ < \\ \text{choose } H_0 \end{array} \tilde{\gamma}, \quad (5.2)$$

where

$$g_i(\rho) = g_1(\rho_1, \rho_2) = -\frac{f'_w(\rho_1)}{f_w(\rho_1)} + a \frac{f'_w(\rho_2 - a\rho_1)}{f_w(\rho_2 - a\rho_1)}, \quad (5.3)$$

for  $i = 1$ ,

$$g_i(\rho) = g_i(\rho_{i-1}, \rho_i, \rho_{i+1}) = -\frac{f'_w(\rho_i - a\rho_{i-1})}{f_w(\rho_i - a\rho_{i-1})} + a \frac{f'_w(\rho_{i+1} - a\rho_i)}{f_w(\rho_{i+1} - a\rho_i)}, \quad (5.4)$$

for  $i = 2, \dots, N-1$ , and

$$g_i(\rho) = g_N(\rho_{N-1}, \rho_N) = -\frac{f'_w(\rho_N - a\rho_{N-1})}{f_w(\rho_N - a\rho_{N-1})}, \quad (5.5)$$

for  $i = N$ , where  $f_w(\cdot)$  is the pdf of  $w_i$ .

The expressions in Eq. (5.3), Eq. (5.4), and Eq. (5.5) illustrate how the use of the AR noise model reduces the LO nonlinearity from a function of an  $N$ -dimensional pdf to functions of a 1-dimensional pdf, the pdf of the iid noise samples,  $\{w_i\}$ . Furthermore, the enhancement techniques derived and discussed in this report may prove useful as means for estimating the driving white noise pdf,  $f_w(\cdot)$ , reliably and accurately, thereby improving performance relative to standard large  $J/S$  implementations. Before a viable LO detector for AR noise can be implemented, however, a number of

issues must be addressed. These include: (1) deriving *robust* LO detector algorithms for AR noise, (2) identifying techniques, such as the Yule-Walker and Burg methods [20], for estimating the coefficients of the AR process, and (3) determining methods for estimating the driving white noise pdf,  $f_w(\cdot)$ , of the AR process. Once these issues are resolved, the use of AR modeling to specify the structure of the robust LO detector has the potential to significantly augment the existing detector methods for use in more complex interference environments.

# Bibliography

- [1] J. Capon, "On the Asymptotic Efficiency of Locally Optimum Detectors," *IRE Transactions on Information Theory*, pp. 67-71, April 1961.
- [2] D. Middleton, "Canonically Optimum Threshold Detection," *IEEE Transactions on Information Theory*, Vol. IT -12, No. 2, pp. 230-243, April 1966.
- [3] W. Gardner, "Structural Characterization of Locally Optimum Detectors in Terms of Locally Optimum Estimators and Correlators," *IEEE Transactions on Information Theory*, Vol. IT-28, No. 6, pp. 924-932, November 1982.
- [4] S. A. Kassam, *Signal Detection in Non-Gaussian Noise*, New York: Springer-Verlag, 1988.
- [5] D. R. Ucci, W. E. Jacklin, and J. G. Grimm, *Investigation and Simulation of Nonlinear Processors for Spread Spectrum Receivers*, Final Technical Report for Rome Laboratory, USAF, Report No. RL-TR-93-258, 1993.
- [6] W. E. Jacklin, J. H. Grimm, and D. R. Ucci, "The Simulation of a Two-Dimensional Spread Spectrum System with Locally Optimal Processing," *Proceedings of the 1993 IEEE MILCOM Conference*, pp. 288-292, 1993.
- [7] J. H. Grimm, et. al., "Continuous Polynomial Approximation," *Proceedings of the 1993 IEEE MILCOM Conference*, pp. 283-287, October 1993.

- [8] D. R. Ucci, W. E. Jacklin, and J. G. Grimm, *A Spread Spectrum Receiver with Nonlinear Processing*, Final Technical Report for Rome Laboratory, USAF, Report No. RL-TR-93-50, 1993.
- [9] Hazeltine Report No. 6662, *Adaptive Nonlinear Coherent Processor Design*, Final Technical Report for Rome Air Development Center, USAF, Report No. RADC-TR-89-387, 1990. \*
- [10] J. H. Higbie, "Adaptive Nonlinear Suppression of Interference," *Proceedings of the 1988 IEEE MILCOM Conference*, pp. 23.3.1-9, 1988.
- [11] J. G. Proakis, *Digital Communications*, Second Edition, New York: McGraw-Hill, 1989.
- [12] D. R. Ucci, W. E. Jacklin, and J. Tamas, *Quasi-optimal Processing in Spread Spectrum Environments*, Final Technical Report for Rome Laboratory, USAF, RL Contract No. F30602-93-C-0099, 1994.
- [13] Melsa, J. L. and Cohn, D. L., *Decision and Estimation Theory*, McGraw-Hill, Inc., 1978.
- [14] W. E. Jacklin and D. R. Ucci, "The Fourier Series Implementation of a Locally Optimum Detector," *Proceedings of the 1994 IEEE MILCOM Conference*, pp. 992-996, October 1994.
- [15] D. W. Scott, *Multivariate Density Estimation: Theory, Practice, and Visualization*, New York: John Wiley and Sons, 1992.
- [16] H. Stark and J. Woods, *Probability, Random Processes, and Estimation Theory for Engineers*, Second Edition, Englewood Cliffs, NJ: Prentice-Hall, 1994.
- [17] M. A. Munem and D. J. Foulis, *Calculus with Analytic Geometry*, Second Edition, New York: Worth Publishers, Inc., 1984.
- [18] J. G. Proakis and D. G. Manolakis, *Introduction to Digital Signal Processing*, New York: Macmillan Publishing Company, 1988.
- [19] P. M. Clarkson and H. Stark, eds., *Signal Processing Methods for Audio, Images and Telecommunications*, London: Academic Press, 1995.

\*Although this report references the limited document noted above, no limited information has been extracted. DOD and DOD contractors only; premature dissemination; to protect information on systems or hardware in the development or concept stage; Mar 90.



- [20] Clarkson, P. M., *Optimal and Adaptive Signal Processing*, CRC Press, Inc., 1993.